

**Radiative Corrections to the Muonium Hyperfine Structure.****I. The  $\alpha^2(Z\alpha)$  Correction**T. Kinoshita\* and M. Nio<sup>† ‡</sup>*Newman Laboratory of Nuclear Studies, Cornell University, Ithaca, NY 14853*

(February 1, 2008)

**Abstract**

This is the first of a series of papers on a systematic application of the NRQED bound state theory of Caswell and Lepage to higher-order radiative corrections to the hyperfine structure of the muonium ground state. This paper describes the calculation of the  $\alpha^2(Z\alpha)$  radiative correction. Our result for the complete  $\alpha^2(Z\alpha)$  correction is 0.424(4) kHz, which reduces the theoretical uncertainty significantly. The remaining uncertainty is dominated by that of the numerical evaluation of the nonlogarithmic part of the  $\alpha(Z\alpha)^2$  term and logarithmic terms of order  $\alpha^4$ . These terms will be treated in the subsequent papers.

PACS numbers: 36.10.Dr, 12.20.Ds, 31.30.Jv, 06.20.Jr

Typeset using REVTeX

---

\*e-mail: tk@hepth.cornell.edu

<sup>†</sup>e-mail: makiko@pa.uky.edu

<sup>‡</sup>present address: Department of Physics and Astronomy, University of Kentucky, Lexington, KY

## I. INTRODUCTION

The hyperfine structure of hydrogenic atoms is one of the well-understood problems both experimentally and theoretically. Especially, the muonium has played an important role in the precision test of QED because its radiative corrections have been calculated to high orders and its hyperfine splitting has been measured very precisely [1]:

$$\Delta\nu(\text{exp}) = 4\,463\,302.88\,(16)\,\text{kHz} \quad (0.036\,\text{ppm}). \quad (1)$$

Furthermore, a new experiment is in progress to improve the precision of  $\Delta\nu(\text{exp})$  to about 0.007 ppm [2]. To match this experimental accuracy, it is necessary to improve the theory of the  $\alpha^2(Z\alpha)$  and  $\alpha(Z\alpha)^2$  non-recoil radiative corrections as well as the leading  $\ln(Z\alpha)$  terms of order  $\alpha^{4-n}(Z\alpha)^n$ ,  $n = 1, 2, 3$ , and some relativistic corrections. This paper presents details of the calculation of the  $\alpha^2(Z\alpha)$  radiative correction. A preliminary report of this work has been published [3].

As is well known, the bulk of the hyperfine splitting can be explained by the nonrelativistic quantum mechanics and is given by the Fermi formula [4]

$$E_F = \frac{16}{3}\alpha^2 c R_\infty \frac{m}{M} \left[1 + \frac{m}{M}\right]^{-3}, \quad (2)$$

where  $R_\infty$  is the Rydberg constant for infinite nuclear mass, and  $m$  and  $M$  are the electron and muon masses, respectively.

Many correction terms have been calculated over several decades since the pioneering work of Fermi. Unfortunately, different terms were often evaluated by different methods making comparison of the results nontrivial in some cases. This causes a particularly difficult problem in identifying and evaluating higher order correction terms. Recently, however, Lepage and his collaborators have developed an approach, called NRQED, to deal with the nonrelativistic and weakly coupled bound systems consistently, starting from quantum electrodynamics (QED) [5–7]. This provides a solid framework for evaluating higher order radiative corrections systematically and unambiguously. This series of papers deal with a

treatment of radiative corrections of the muonium hyperfine structure within the framework of NRQED.

Before describing our calculation, let us summarize the previous results on the muonium hyperfine splitting  $\Delta\nu$ . It is customary to classify the QED corrections to  $\Delta\nu$  into three types: radiative non-recoil correction, pure recoil correction, and radiative-recoil correction. We use the convention such that electron charge is  $e$  and the charge of the positive muon is  $-Ze$ . Of course  $Z = 1$  for the muon, but it is kept in the formula in order to identify the origin of corrections. Note that each radiative photon on the electron-line contributes a factor  $\alpha$ , that on the muon line a factor  $Z^2\alpha$ , and one jumping from electron to muon a factor  $Z\alpha$ . This factor also arises from the effect of binding on the velocity distribution of atomic electrons. In addition, there are small corrections due to the hadronic vacuum polarization and weak interaction effects. Thus one may write

$$\begin{aligned}\Delta\nu(\text{theory}) = & \Delta\nu(\text{rad}) + \Delta\nu(\text{recoil}) + \Delta\nu(\text{rad-recoil}) \\ & + \Delta\nu(\text{hadron}) + \Delta\nu(\text{weak}).\end{aligned}\tag{3}$$

Purely radiative terms of orders  $\alpha(Z\alpha)$  and  $\alpha(Z\alpha)^2$  have been known for some time [8]:

$$\begin{aligned}\Delta\nu(\text{rad}) = & (1 + a_\mu) \left( 1 + \frac{3}{2}(Z\alpha)^2 + a_e + \alpha(Z\alpha)(\ln 2 - \frac{5}{2}) \right. \\ & - \frac{8\alpha(Z\alpha)^2}{3\pi} \ln(Z\alpha) \left[ \ln(Z\alpha) - \ln 4 + \frac{281}{480} \right] \\ & \left. + \frac{\alpha(Z\alpha)^2}{\pi} (14.88 \pm 0.29) \right) E_F.\end{aligned}\tag{4}$$

Here  $a_e$  and  $a_\mu$  are the anomalous magnetic moments of the electron and muon, respectively. The appearance of the factor  $(1 + a_\mu)$  in (4) is in accord with our definition of  $E_F$  in (2). Note that the number 14.88 in the  $\alpha(Z\alpha)^2$  correction is different from 15.39 reported in Ref. [8]. This is due to the recent discovery of two mistakes in the literature. The first error is in the calculation of the  $\alpha(Z\alpha)^2$  correction due to the vacuum polarization insertion in the transverse photon in Ref. [9]. Recently several people independently found [10–12] that this contribution is  $E_F\alpha(Z\alpha)^2/\pi(-4/5)$ , not  $E_F\alpha(Z\alpha)^2/\pi(-2/3)$  given in Ref. [9]. The second

error was caused by omission of a part of the contribution due to the vacuum polarization insertion in the Coulomb photon,  $E_F\alpha(Z\alpha)^2/\pi(-8/15)\ln 2$ , when it was combined with the radiative photon contribution  $E_F\alpha(Z\alpha)^2/\pi(15.10 \pm 0.29)$  [11].

The known recoil corrections add up to [8]

$$\Delta\nu(\text{recoil}) = \left( -\frac{3Z\alpha}{\pi} \frac{mM}{M^2 - m^2} \ln \frac{M}{m} + \frac{\gamma^2}{mM} \left[ 2 \ln \frac{m_r}{2\gamma} - 6 \ln 2 + \frac{65}{18} \right] \right) E_F, \quad (5)$$

where  $\gamma \equiv Z\alpha m_r$ ,  $m_r = mM/(m+M)$ . The radiative-recoil contributions, which arise from both electron and muon lines and from vacuum polarizations, are given by <sup>1</sup>

$$\begin{aligned} \Delta\nu(\text{rad-recoil}) = & \frac{\alpha(Z\alpha)}{\pi^2} \frac{m}{M} \left( -2 \ln^2 \frac{M}{m} + \frac{13}{12} \ln \frac{M}{m} + 6\zeta(3) + \zeta(2) - \frac{71}{72} + 3\pi^2 \ln 2 \right. \\ & + Z^2 \left[ \frac{9}{2} \zeta(3) + \frac{39}{8} - 3\pi^2 \ln 2 \right] \\ & \left. + \frac{\alpha}{\pi} \left[ -\frac{4}{3} \ln^3 \frac{M}{m} + \frac{4}{3} \ln^2 \frac{M}{m} + \mathcal{O} \left( \ln \frac{M}{m} \right) \right] \right) E_F. \end{aligned} \quad (6)$$

The  $\alpha(Z\alpha)(m/M)$  and  $Z^2\alpha(Z\alpha)(m/M)$  terms are known exactly [8,13]. The  $\ln^3$  and  $\ln^2$  parts of the  $\alpha^2(Z\alpha)$  term were evaluated by Eides *et al.* [14].

The hadronic vacuum polarization contributes [15]

$$\begin{aligned} \Delta\nu(\text{hadron}) &= \frac{\alpha(Z\alpha)}{\pi^2} \frac{mM}{m_\pi^2} (3.75 \pm 0.24) E_F \\ &= 0.250 \text{ (16) kHz}, \end{aligned} \quad (7)$$

where  $m_\pi$  is the charged pion mass.

Finally there is a small contribution due to the  $Z^0$  exchange. Our re-evaluation of the standard-model estimate [16,17] gives <sup>2</sup>

---

<sup>1</sup>Eq. (6) of Ref. [3] is valid only for  $Z = 1$  although it does not affect the muonium. We thank B. N. Taylor and P. Mohr for pointing out this oversight.

<sup>2</sup> This is in agreement with the corrected value given in Ref. [17] and has a sign opposite to that of Ref. [3]. The same result was also obtained by J. R. Sapirstein and by M. I. Eides. We thank B. N. Taylor and P. Mohr for calling a possible problem of sign to our attention.

TABLE I. Contributions of various terms to the hyperfine splitting of the ground state muonium. (The new result of this paper is not included.) They are represented in units of kHz. The contribution from the muon anomalous magnetic moment is included in each non-recoil radiative correction term in the left column.

term	kHz	term	kHz
$E_F$	4 459 032.409	$Z\alpha m/M$	-800.304
$a_e$	5 170.927	$(Z\alpha)^2 m/M$	8.982
$(Z\alpha)^2$	356.174	$\alpha(Z\alpha)m/M$	-2.636
$\alpha(Z\alpha)$	-429.036	$Z^2\alpha(Z\alpha)m/M$	-1.190
$\alpha(Z\alpha)^2 \ln^2(Z\alpha)^{-1}$	-35.606	$\alpha^2(Z\alpha)m/M$	-0.044
$\alpha(Z\alpha)^2 \ln(Z\alpha)^{-1}$	-5.796	hadron	0.250
$\alpha(Z\alpha)^2$	8.207	weak	-0.065

$$\begin{aligned}\Delta\nu(\text{weak}) &= -G_F \frac{3\sqrt{2}mM}{8\alpha\pi} E_F \\ &\simeq -0.065 \text{ kHz.}\end{aligned}\tag{8}$$

Numerical values of terms given by Eqs. (4) - (8) are summarized in Table I. If one uses the value of  $\alpha$ ,  $R_\infty$  and  $M/m$  from Refs. [18], [19] and [1]:

$$\begin{aligned}\alpha^{-1} &= 137.035\,997\,9\,(32) \quad (0.024 \text{ ppm}) \\ R_\infty &= 10\,973\,731.568\,30\,(31) \text{ m}^{-1}, \\ \frac{M}{m} &= 206.768\,259\,(62),\end{aligned}\tag{9}$$

theoretical prediction for the hyperfine splitting of the ground state muonium, sum of the contributions listed in Table I, is given by

$$\Delta\nu(\text{old theory}) = 4\,463\,302.27\,(1.34)\,(0.21)\,(0.16)\,(1.00)\tag{10}$$

where the first and second errors reflect the uncertainties in the measurements of  $m_\mu$  and

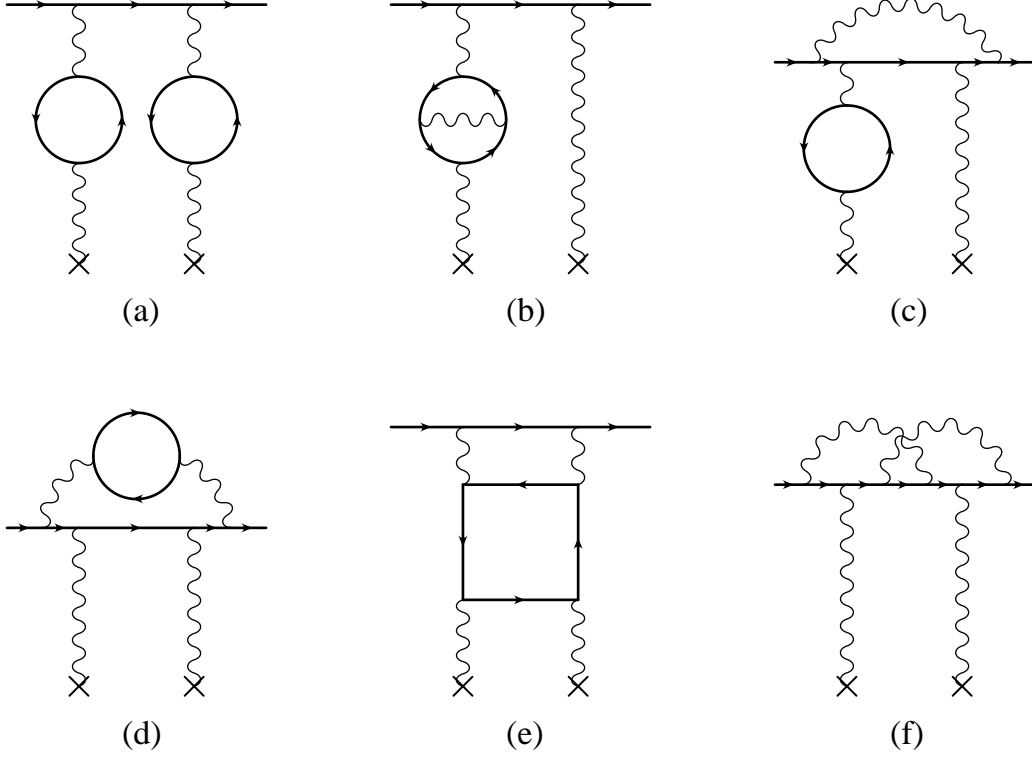


FIG. 1. Representative diagrams contributing to the  $\alpha^2(Z\alpha)$  radiative corrections to the muonium hyperfine structure in which two virtual photons are exchanged between  $e^-$  and  $\mu^+$ . The muon is represented by  $\times$ .

$\alpha^{-1}$  listed in (9). The third error is purely theoretical and dominated by the uncertainty in the last  $\alpha(Z\alpha)^2$  term of (4). The last one, about 1 kHz, is an estimated contribution from the order  $\alpha^2(Z\alpha)$  correction in  $\Delta(\text{rad})$ .

As is clear from (10) one must know the  $\alpha^2(Z\alpha)$  pure radiative correction in order to improve the theoretical prediction further. Fig. 1 shows typical diagrams contributing to this order. Recently, terms represented by the diagrams (a) - (e) of Fig. 1 have been evaluated by Eides *et al.* [20]. Their results are as follows:

$$\begin{aligned}\Delta\nu(\text{Fig.1(a)}) &= \frac{36}{35} \frac{\alpha^2(Z\alpha)}{\pi} E_F \\ &= 0.567 \text{ 3 kHz},\end{aligned}\tag{11}$$

$$\Delta\nu(\text{Fig.1(b)}) = \left( \frac{224}{15} \ln 2 - \frac{38}{15} \pi - \frac{118}{225} \right) \frac{\alpha^2(Z\alpha)}{\pi} E_F$$

$$= 1.030 \text{ 2 kHz}, \quad (12)$$

$$\begin{aligned} \Delta\nu(\text{Fig.1(c)}) &= \left( -\frac{4}{3}z^2 - \frac{20\sqrt{5}}{9}z - \frac{64}{45}\ln 2 + \frac{\pi^2}{9} + \frac{1043}{675} + \frac{3}{8} \right) \frac{\alpha^2(Z\alpha)}{\pi} E_F \\ &= -0.368 \text{ 9 kHz}, \end{aligned} \quad (13)$$

$$\begin{aligned} \Delta\nu(\text{Fig.1(d)}) &= -0.310 \text{ 742} \dots \frac{\alpha^2(Z\alpha)}{\pi} E_F \\ &= -0.171 \text{ 4 kHz}, \end{aligned} \quad (14)$$

where  $z = \ln((1 + \sqrt{5})/2)$ . The results (11), (12) and (13) are analytic, while (14) was evaluated numerically after reducing the integral to one dimension. We confirmed these results by an independent numerical calculation. However, our purely numerical evaluation of Fig. 1(e):

$$\begin{aligned} \Delta\nu(\text{Fig.1(e)}) &= -0.472 \text{ 48 (9)} \frac{\alpha^2(Z\alpha)}{\pi} E_F \\ &= -0.260 \text{ 6 kHz} \end{aligned} \quad (15)$$

disagreed with the semi-analytic result of Ref. [21]. With our help, Eides [22] found an error in the Table after Eq. (23) of Ref. [21]. Their corrected value is in good agreement with (15).

Fig. 2 shows the complete set of Feynman diagrams of the type (f) of Fig. 1, which have not been evaluated before our work [3]. The preliminary result of our calculation for all diagrams of Fig. 2 was

$$\begin{aligned} \Delta\nu(\text{Fig.1(f)}) &= -0.63 \text{ (4)} \frac{\alpha^2(Z\alpha)}{\pi} E_F \\ &= -0.347 \text{ (22) kHz}, \end{aligned} \quad (16)$$

where the error is mainly due to the uncertainty in extrapolating the integral to zero infrared cutoff. The main purpose of this paper is to report a further improvement of this result:

$$\begin{aligned} \Delta\nu(\text{Fig.1(f)}) &= -0.676 \text{ 4 (79)} \frac{\alpha^2(Z\alpha)}{\pi} E_F \\ &= -0.373 \text{ 1 (44) kHz}. \end{aligned} \quad (17)$$

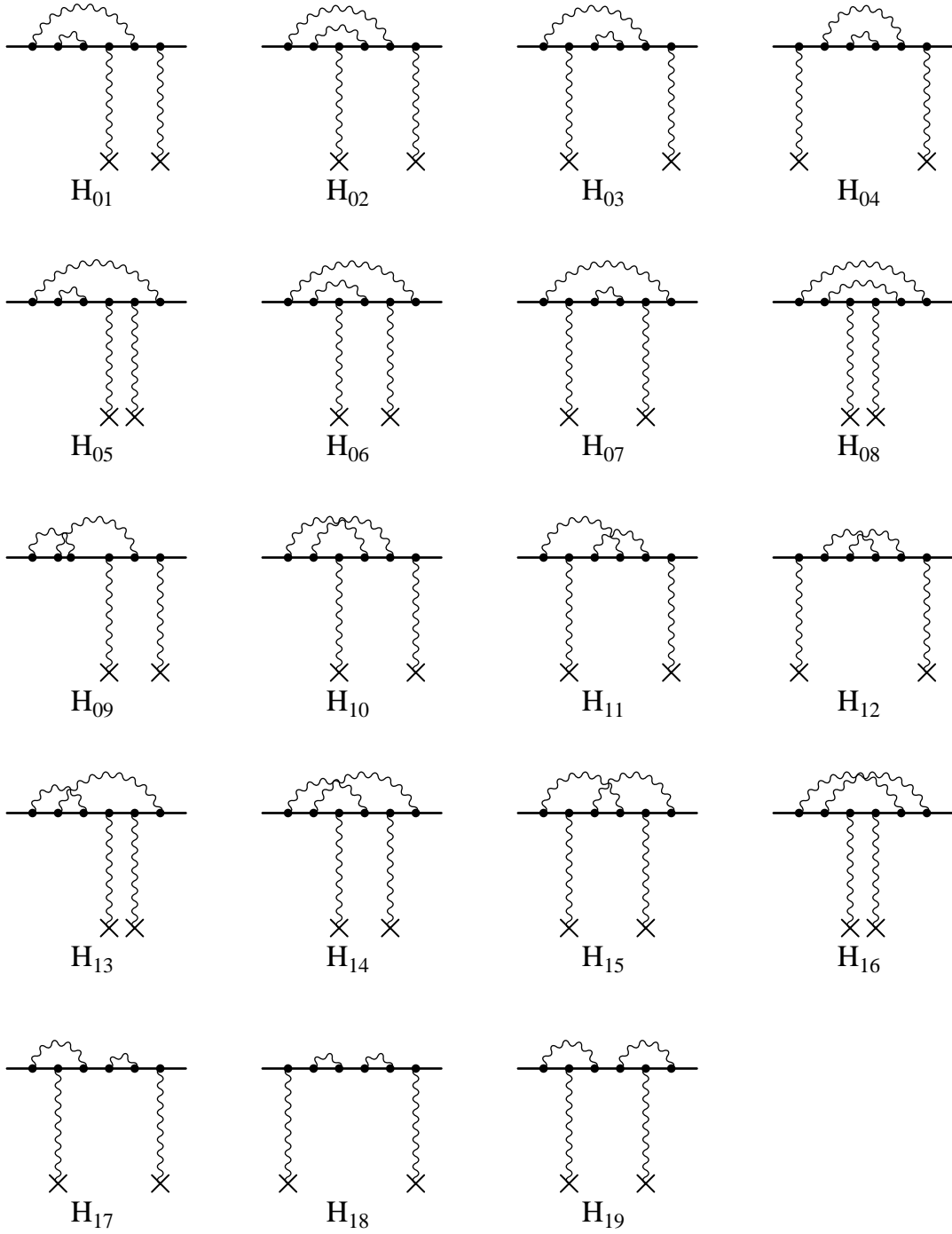


FIG. 2. Two-photon exchange diagrams with fourth-order radiative corrections on the electron-line. Diagrams which are related to these diagrams by time reversal are not shown explicitly. The muon is represented by  $\times$ .



As a consequence of this result, the total contribution of the  $\alpha^2(Z\alpha)$  correction to the muonium hyperfine splitting becomes

$$\begin{aligned}\Delta\nu(\text{Fig.1}) &= 0.767\,9\,(79)\frac{\alpha^2(Z\alpha)}{\pi}E_F \\ &= 0.423\,5\,(44)\,\text{kHz}.\end{aligned}\tag{18}$$

This removes the dominant theoretical uncertainty in  $\Delta\nu(\text{theory})$ .

In Sec. II we outline the NRQED treatment of two-body bound system. It serves as the theoretical basis for the calculation of the  $\alpha^2(Z\alpha)$  correction as well as the calculation of the  $\alpha(Z\alpha)^2$  and higher order corrections discussed in the subsequent papers. In Sec. III we illustrate the general procedure of NRQED choosing the well-known  $\alpha(Z\alpha)$  non-recoil radiative correction as an example. In Sec. IV we present our calculation of the  $\alpha^2(Z\alpha)$  purely radiative non-recoil correction to the muonium hyperfine structure. Some problems encountered in the numerical work are also discussed there. Sec. V is devoted to the discussion of our results.

## II. NRQED

### A. Why NRQED ?

The Lorentz invariance has been one of the most important guiding principles for the development of quantum field theory. However, relativistic quantum field theory is often very cumbersome to apply to nonrelativistic bound systems. Such a calculation tends to be very complicated and requires an enormous effort, while the result reflects mostly the nonrelativistic feature of the system. For such a system an approach that incorporates most of the bound state effects from the beginning would minimize the amount of computation necessary to achieve the desired precision. For the case of electromagnetic interaction, this has been realized by a theory called nonrelativistic quantum electrodynamics, or NRQED. The NRQED enables us to avoid some, if not all, of the problems encountered in the usual treatment based on the Bethe-Salpeter equation.

The NRQED, formulated by Caswell and Lepage [5], is a rigorous adaptation of QED to bound systems. This theory enables us to take a consistent and systematic approach to loosely bound nonrelativistic systems. Compared with the conventional bound state theories, it allows easier power counting, more transparent cancellation of UV and IR divergences, and is manifestly gauge invariant. In spite of its superiority, however, the details of the theory has not yet been fully worked out. In this series of papers, we present an explicit construction of the NRQED Hamiltonian and develop a bound state perturbation theory based on it.

As for the computation of the  $\alpha(Z\alpha)$  and  $\alpha^2(Z\alpha)$  corrections, NRQED or any other relativistic bound state formalism gives the same simple recipe: calculate the forward scattering amplitude in QED and multiply it with  $|\phi(0)|^2$ , where  $\phi(0)$  is the nonrelativistic wave function at the origin. In NRQED this recipe can be directly justified by inspection of relevant diagrams and power counting. In other bound state formalisms, the corresponding procedure may be less straightforward. The latter approach becomes very complicated for higher-order corrections such as the  $\alpha(Z\alpha)^2$  and  $\alpha(Z\alpha)^3$  corrections. Difficulty in achieving high numerical precision by this method is one of the sources of theoretical uncertainty at present [8,23].

The approach adopted by the NRQED, however, loses its effectiveness for the high  $Z$  system. In such a case it is desirable to avoid expanding in  $v \sim Z\alpha$ . Recently, an attempt has been made to calculate the order  $\alpha$  term without expanding in  $Z\alpha$  [24]. However, this approach may have difficulty in providing a good precision for  $Z = 1$ . This is primarily because, for low  $Z$  systems, the bound electron is almost on-the-mass-shell and causes the near infrared divergence. As a consequence the convergence of numerical integration deteriorates as  $Z$  decreases. As is shown in the subsequent papers, the NRQED method enables us to deal with the near infrared divergence problem order by order in a systematic expansion in  $Z\alpha$ , and allows us to calculate the expansion coefficients with high precision. This is why the NRQED method is a powerful tool for low  $Z$  systems.

## B. Outline of NRQED

In the NRQED approach to the bound state problem, one first derives the NRQED Lagrangian from the QED, and then uses it to determine the correction to the energies and wave functions by a systematic application of the Rayleigh-Schrödinger perturbation theory.

The NRQED Lagrangian consists of all possible local interactions satisfying the required symmetries, such as gauge invariance, parity invariance, time reversal, galileian invariance, hermiticity, and locality. We use the same photon Lagrangian  $(-1/4)F_{\mu\nu}F^{\mu\nu}$  as that of QED. In addition, new photon interaction terms are introduced to represent the insertion of the fermion loop, such as vacuum polarization and light-by-light scattering.

In order to define the NRQED Lagrangian precisely, we must regularize the interaction terms of NRQED, e.g., by cutting off contributions of large momenta. Since this theory is meant to apply to nonrelativistic systems, the cut-off  $\Lambda$  may be chosen as the typical mass scale of the system, e.g., the rest mass of an electron. With the cut-off  $\Lambda$  thus fixed, the theory becomes well-defined, even though the interaction terms are strongly dependent on the cut-off parameter. In the following the cut-off is understood implicitly, and will be exhibited only when it is necessary. The choice of the momentum cut-off used for the NRQED scattering amplitudes is arbitrary but the physical quantity computed should be independent of any particular choice. In other words, the NRQED theory must have reparametrization invariance with respect to the choice of cut-off. This is analogous to the existence of the renormalization group in the renormalizable relativistic field theory. It is important to note that the NRQED is fully equivalent to the QED. The only difference is that it is better adapted to low energy bound systems.

The NRQED rule for determining the operators which appear in its Lagrangian and their coefficients is simple and straightforward: Each term of the *scattering* amplitude calculated in the NRQED must coincide with the corresponding *scattering* amplitude of the original QED at some given momentum scale, e.g., at the threshold of the external on-shell particles. The center of mass frame is used for both bound state and scattering state calculations. Since

the same argument about reparametrization invariance holds for the momentum scale chosen for comparison of QED and NRQED scattering amplitudes, the at-threshold condition is just for convenience. However, the on-shell condition for the external fermion is more than a matter of convenience. In order to regulate the IR singularity it is convenient to introduce the photon mass  $\lambda$  in the calculation of scattering amplitude of both QED and NRQED. This finite photon mass together with the on-shell condition ensures that the NRQED scattering theory has a pole in the region of the complex energy plane of the external fermion in which the scattering theory can be analytically continued to the off-shell bound state theory.

We use the normalization  $u^\dagger u = 1$  for the external 4-component spinors in the QED calculation instead of the conventional relativistic normalization  $\bar{u}u = 1$  so that both QED and NRQED  $S$ -matrix have the same normalization [25]. This ensures that physical quantities, such as decay rate and cross section, calculated in both theories are the same.

Note that the scattering amplitude of QED is fully renormalized, namely, it is finite and completely determined within QED. This enables us to fix the NRQED “renormalization” constants without ambiguity. This also means that the coupling constant  $\alpha$  and fermion masses in the QED are the renormalized ones determined on-shell, and these  $\alpha$  and fermion masses are used as the “bare” coupling constant and “bare” masses of NRQED.

It is convenient to write the NRQED Lagrangian in two parts:  $L_{\text{main}}$  and  $L_{\text{contact}}$ . The  $L_{\text{main}}$  part consists of the fermion bilinear operators. Fermions in NRQED are expressed by the Pauli two component spinor field  $\psi(t, \vec{x})$  (instead of the Dirac spinor). If one takes into account the required symmetries of the theory, the main part of NRQED Lagrangian  $L_{\text{main}}$  must have the general form [5,6]

$$\begin{aligned}
L_{\text{main}} = \psi^\dagger \{ & iD_t + \frac{\vec{D}^2}{2m} + \frac{\vec{D}^4}{8m^3} \\
& + c_F \frac{e\vec{\sigma} \cdot \vec{B}}{2m} + c_D \frac{e(\vec{D} \cdot \vec{E} - \vec{E} \cdot \vec{D})}{8m^2} \\
& + c_S \frac{ie\vec{\sigma} \cdot (\vec{D} \times \vec{E} - \vec{E} \times \vec{D})}{8m^2} + c_{W1} \frac{e\{\vec{D}^2, \vec{\sigma} \cdot \vec{B}\}}{8m^3} \\
& + c_{W2} \frac{-e\vec{D}^i \vec{\sigma} \cdot \vec{B} \vec{D}^i}{4m^3} + c_{p'p} \frac{e(\vec{\sigma} \cdot \vec{D} \vec{B} \cdot \vec{D} + \vec{D} \cdot \vec{B} \vec{\sigma} \cdot \vec{D})}{8m^3} + \dots \} \psi .
\end{aligned} \tag{19}$$

where  $D_t = \partial_t + ieA^0$  and  $\vec{D} = \vec{\partial} - ie\vec{A}$ . (We put  $c = 1$  and  $\hbar = 1$  henceforth.) The positron part can be written down in a similar way. The particle-antiparticle mixed interaction is not present in  $L_{\text{main}}$ . The first three terms are related to the kinetic term of the QED Lagrangian. The second and third terms are derived from the expansion

$$E = \sqrt{\vec{p}^2 + m^2} = m + \frac{\vec{p}^2}{2m} - \frac{\vec{p}^4}{8m^3} + \dots \quad (20)$$

These three terms of (19) have coefficients unaffected by the radiative correction as a consequence of the renormalizability of QED, while the coefficients  $c_i$  of other terms are modified by the QED interaction and can be expressed as a power series in the coupling constants  $\alpha$

$$c_i = c_i^{(0)} + c_i^{(1)}\alpha + c_i^{(2)}\alpha^2 + \dots \quad (21)$$

Some of the operators in (19) can be generated by the Foldy-Wouthuysen-Tani transformation of the Dirac Lagrangian. These operators have the coefficient  $c_i^{(0)} = 1$  while other operators have  $c_i^{(0)} = 0$ . Note that  $c_i$ 's do not have coefficients involving  $Z\alpha$  caused by the binding effect because they are determined solely by comparison of the NRQED and QED *scattering* amplitudes without referring to the bound states.

Eq. (19) has an infinite number of terms. Not all of them, of course, are needed in a practical calculation. The operators necessary to carry out a particular calculation are determined by the power counting rule of NRQED for the bound state. We will show this process explicitly in the next subsections where the NRQED Hamiltonian is constructed.

The  $L_{\text{main}}$  of NRQED alone is not sufficient to produce the same physical quantities as those from QED. To make NRQED equivalent to QED, we must add another term to the NRQED Lagrangian. It consists of terms of contact interaction type:

$$\begin{aligned} L_{\text{contact}} = & d_1 \frac{1}{mM} (\psi^\dagger \vec{\sigma} \psi) \cdot (\chi^\dagger \vec{\sigma} \chi) + d_2 \frac{1}{mM} (\psi^\dagger \psi) (\chi^\dagger \chi) \\ & + d_3 \frac{1}{mM} (\psi^\dagger \vec{\sigma} \chi) \cdot (\chi^\dagger \vec{\sigma} \psi) + d_4 \frac{1}{mM} (\psi^\dagger \chi) (\chi^\dagger \psi) \\ & + d_5 \frac{1}{m^3 M} (\psi^\dagger \vec{D}^2 \vec{\sigma} \psi) \cdot (\chi^\dagger \vec{\sigma} \chi) + \dots \quad , \end{aligned} \quad (22)$$

where  $\chi$  represents a fermion field (of mass  $M$ ) such as a muon or a positron. The third and fourth terms in (22) are needed only when both electron and positron are present. This is

because, from the viewpoint of NRQED, the electron-positron annihilation is a high energy process and can only be represented as a contact interaction term. For the muonium, only the first and second terms are relevant. The fifth term is an example of contact terms including derivative interactions, which are of higher order in  $\langle \vec{p}^2/m^2 \rangle \sim (Z\alpha)^2$ .

The coefficients  $d_i$  are chosen such that these contact interactions make up the difference between the QED electron-muon scattering amplitude and the corresponding NRQED scattering amplitude derived from the Lagrangian  $L_{\text{main}}$ . This procedure enables us to determine the coefficients  $d_i$  completely.

As is clear from the above discussion, these NRQED “renormalization” constants  $c_i$  and  $d_i$  have the parameter dependence

$$\begin{aligned} c_i &= c_i(\alpha, \Lambda, m), \\ d_i &= d_i(\alpha, Z\alpha, Z^2\alpha, \Lambda, m, M). \end{aligned} \tag{23}$$

Of course, the experimentally observable result of calculation must be independent of the cut-off  $\Lambda$ , and gauge invariant. This is realized by a systematic application of the nonrelativistic Rayleigh-Schrödinger perturbation theory to the bound states. Note also that  $c_i$  and  $d_i$  are finite and well-defined in the infrared limit and hence require no infrared cut-off.

Just as the actual execution of renormalization program of QED must rely on the covariant perturbation theory, a comprehensive formulation of NRQED can be realized explicitly only within the framework of the nonrelativistic Rayleigh-Schrödinger perturbation theory. This means that we have to choose an appropriate part of the Hamiltonian as the unperturbed term and treat the rest as perturbation.

To deal with the muonium we find it generally convenient to define the unperturbed system in terms of the ground state solution of the nonrelativistic Schrödinger equation:

$$\left( \frac{\vec{p}^2}{2m_r} - \frac{Z\alpha}{r} \right) \phi = E^0 \phi, \tag{24}$$

where  $m_r$  is the reduced mass,  $E^0 = -\gamma^2/(2m_r)$  is the ground state binding energy,  $\gamma \equiv (Z\alpha)m_r$  being a typical momentum scale of the Coulomb bound state. The solution of this equation is

$$\phi(\vec{p}) = \frac{8\sqrt{\pi}\gamma^5}{(\vec{p}^2 + \gamma^2)^2} . \quad (25)$$

The unperturbed electron field  $\psi(\vec{p})$  is thus expressed by this wave function  $\phi(\vec{p})$  times the Pauli spin factor. Using the remaining interaction terms in the NRQED Lagrangian together with the photon Lagrangian, we can construct the effective potentials. These potentials are to be treated as perturbation.

The nonrelativistic Rayleigh-Schrödinger perturbation theory gives

$$\begin{aligned} \Delta E_n &= \psi_n^\dagger V \psi_n [1 + \psi_n^\dagger \left( \frac{\partial}{\partial E} V \right) \psi_n]_{E=E_n^0} \\ &+ \psi_n^\dagger V (\tilde{G}_0 - \frac{\psi_n \psi_n^\dagger}{E - E_n^0}) V \psi_n \big|_{E=E_n^0} \\ &+ \psi_n^\dagger V (\tilde{G}_0 - \frac{\psi_n \psi_n^\dagger}{E - E_n^0}) V (\tilde{G}_0 - \frac{\psi_n \psi_n^\dagger}{E - E_n^0}) V \psi_n \big|_{E=E_n^0} \\ &+ \psi_n^\dagger V \psi_n \psi_n^\dagger \left( \frac{\partial}{\partial E} \left( V (\tilde{G}_0 - \frac{\psi_n \psi_n^\dagger}{E - E_n^0}) V \right) \right) \psi_n \big|_{E=E_n^0} \\ &+ \dots \end{aligned} \quad (26)$$

The Green function  $\tilde{G}_0(\vec{k}, \vec{q} : E_n^0)$  appearing here is known in a closed form for the nonrelativistic Coulomb potential [26]. For the ground state  $n = 1$ , we find

$$\begin{aligned} \lim_{E \rightarrow E_{n=1}^0} (\tilde{G}_0 - \frac{\psi_{n=1} \psi_{n=1}^\dagger}{E - E_{n=1}^0}) &= \frac{-2m_r}{\vec{k}^2 + \gamma^2} (2\pi)^3 \delta^3(\vec{k} - \vec{q}) \\ &+ \frac{-2m_r}{(\vec{k}^2 + \gamma^2)} \frac{-Ze^2}{|\vec{k} - \vec{q}|^2} \frac{-2m_r}{(\vec{q}^2 + \gamma^2)} \\ &- \frac{64\pi}{Z\alpha\gamma^4} \tilde{R}(\vec{k}, \vec{q}) , \end{aligned} \quad (27)$$

where

$$\begin{aligned} \tilde{R}(\vec{k}, \vec{q}) &= \frac{\gamma^8}{(\vec{k}^2 + \gamma^2)^2 (\vec{q}^2 + \gamma^2)^2} \left[ \frac{5}{2} - 4 \frac{\gamma^2}{\vec{k}^2 + \gamma^2} - 4 \frac{\gamma^2}{\vec{q}^2 + \gamma^2} \right. \\ &\quad \left. + \frac{1}{2} \log A + \frac{2A - 1}{(4A - 1)^{1/2}} \tan^{-1}(4A - 1)^{1/2} \right] , \end{aligned} \quad (28)$$

and

$$A = \frac{(\vec{k}^2 + \gamma^2)(\vec{q}^2 + \gamma^2)}{4\gamma^2 |\vec{k} - \vec{q}|^2} . \quad (29)$$

The first, second, and third terms of the expression (27) can be understood as corresponding to zero, one, and two or more Coulomb-photon exchanges.

In order to determine which terms of the Hamiltonian are needed to obtain the desired precision it is useful to know the expectation values of various operators with respect to appropriate wave functions [25]. For a nonrelativistic Coulombic bound system, one finds

$$\begin{aligned} \langle \vec{\partial} \rangle &\sim m(v/c), & \langle \partial_t \rangle &\sim m(v/c)^2, & \langle eA^0 \rangle &\sim m(v/c)^2, \\ \langle e\vec{A} \rangle &\sim m(v/c)^3, & \langle e\vec{E} \rangle &\sim m^2(v/c)^3, & \langle e\vec{B} \rangle &\sim m^2(v/c)^4, \end{aligned} \quad (30)$$

where  $m$  is the electron mass,  $v$  is the typical velocity of a bound electron, and  $c(=1)$  is the velocity of light. Thus, in Eq. (19), the first two terms, next four terms, and the remaining terms correspond to the interactions which start at orders  $v^2$ ,  $v^4$ , and  $v^6$ , respectively. Radiative corrections, which alter the values of the coefficients  $c_i$ 's and  $d_i$ 's, will keep the estimate (30) intact. The information (30) can be used to terminate the series of interaction terms at the desired precision. In this sense, the NRQED Lagrangian is an expansion in both the coupling constant  $\alpha$  and the velocity  $v$ .

The NRQED “renormalization” coefficients play important roles in restoring gauge invariance which might have been broken by regularization. The explicit form of these coefficients depends on the regularization method. Gauge invariant regularization is desirable but not necessary. If one proceeds carefully, even a simple momentum cut-off method may be used [28]. (This is only true for an Abelian gauge theory such as NRQED.) In a calculation of the would-be divergent quantity in NRQED, we put the UV cut-off  $\Lambda$  not in the fermion momentum but in the photon momentum [29].

Because of the way NRQED is constructed, gauge invariance of the NRQED amplitude with its complete set of “renormalization” constants is automatically guaranteed by the gauge invariance of the corresponding QED amplitude. Since QED and NRQED are separately gauge invariant, we may choose different gauges for QED and NRQED. We will use the Feynman gauge for QED calculation, and we use the Coulomb gauge for NRQED. The Feynman gauge minimizes the amount of work for numerical computation, and the Coulomb



gauge is more suitable for describing the nonrelativistic behavior of the electron.

The dominant contribution to the hyperfine splitting between the spin  $J=1$  and  $J=0$  states originates from the interaction between the electron spin and the muon spin mediated by a transverse photon of momentum  $\vec{k}$ . This leads to a potential of the form

$$V_F = \frac{ie}{2m}(\psi^\dagger \vec{k} \times \vec{\sigma}_e \psi) \cdot \frac{-iZe}{2M}(\chi^\dagger(-\vec{k}) \times \vec{\sigma}_\mu \chi) \frac{-1}{\vec{k}^2} \quad (31)$$

in the momentum space representation, where  $M$  is the muon mass. Using this Fermi potential  $V_F$  in the first order perturbation theory and taking the difference between  $J=1$  and  $J=0$  states, we obtain the hyperfine Fermi splitting

$$\begin{aligned} E_F &= \langle n=1 | V_F | n=1 \rangle_{J=0}^{J=1} \\ &= \int \frac{d^3 p}{(2\pi)^3} \int \frac{d^3 k}{(2\pi)^3} \frac{(8\sqrt{\pi}\gamma^5)^2}{(\vec{p}^2 + \gamma^2)^2 (|\vec{p} + \vec{k}|^2 + \gamma^2)^2} \cdot \\ &\quad \frac{ie}{2m} \langle (\vec{k} \times \vec{\sigma}_e) \cdot \frac{-iZe}{2M} ((-\vec{k}) \times \vec{\sigma}_\mu) \rangle \frac{-1}{\vec{k}^2} \\ &= \frac{2(Z\alpha)\gamma^3}{3mM} \langle \vec{\sigma}_e \cdot \vec{\sigma}_\mu \rangle_{J=0}^{J=1} \\ &= \frac{8(Z\alpha)\gamma^3}{3mM} . \end{aligned} \quad (32)$$

Needless to say, the Fermi potential is of order  $v^4(m/M)m \sim (Z\alpha)^4(m/M)m$ .

Various interaction terms and propagators are represented by the NRQED ‘‘Feynman’’ diagrams shown in Fig. 3. It is convenient and useful to express higher-order amplitudes representing scattering states or bound states by corresponding diagrams.

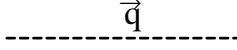
We classify the diagrams according to the number of external photons in the QED Feynman diagrams. In the following subsections we shall show step by step how the corresponding NRQED Lagrangian  $L_{\text{main}}$  (or Hamiltonian  $H_{\text{main}}$ ) is determined.

### C. Scattering by a static external potential

We have already found the general form of the main part of the NRQED Lagrangian given by Eq. (19) using the required symmetries for the theory and the power counting rules.

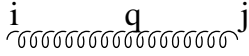
# Propagators

## Coulomb photon propagator



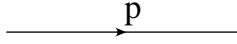
$$\frac{1}{\vec{q}^2 + \lambda^2}$$

## Transverse photon propagator



$$\frac{\delta^{ij} - \frac{q^i q^j}{\vec{q}^2 + \lambda^2}}{(q^0)^2 - \vec{q}^2 - \lambda^2 + i\epsilon}$$

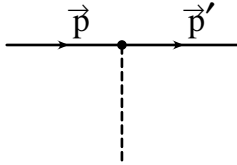
## Fermion propagator



$$\frac{1}{E - \frac{\vec{p}^2}{2m} + i\epsilon}$$

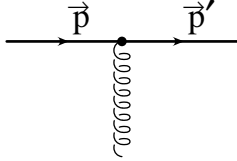
# Vertices

## Coulomb vertex



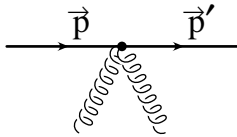
$$e$$

## Dipole vertex



$$-e \frac{\vec{p}' + \vec{p}}{2m}$$

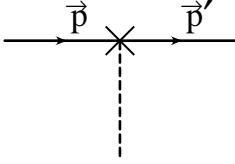
## $\vec{A} \cdot \vec{A}$ vertex



$$\frac{e^2 \delta^{ij}}{2m}$$

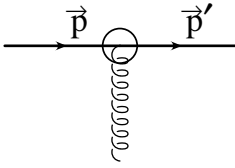
FIG. 3. NRQED “Feynman” rules for vertices and propagators. They can be used for both scattering and bound state calculations.  $E$  in the fermion propagator represents the fermion’s bound state energy:  $E = 0$  for scattering and  $E = -\gamma^2/(2m_r)$  for the ground state muonium. The photon mass  $\lambda$  is set to zero in the bound state calculation.

Figure 3 (continued)



Darwin vertex

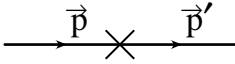
$$\frac{-e}{8m^2} |\vec{p}' - \vec{p}|^2$$



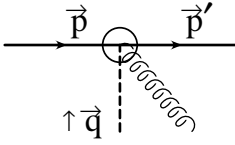
Fermi vertex

$$\frac{ie}{2m} (\vec{p}' - \vec{p}) \times \vec{\sigma}$$

Relativistic kinetic vertex

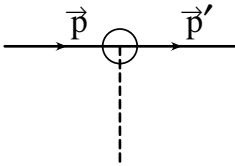


$$\frac{-\vec{p}^4}{8m^3} (2\pi)^3 \delta^3(\vec{p}' - \vec{p})$$



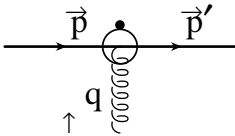
Seagull vertex

$$\frac{ie^2}{4m^2} \vec{q} \times \vec{\sigma}$$



Spin-orbit vertex

$$\frac{ie}{4m^2} (\vec{p}' \times \vec{p}) \cdot \vec{\sigma}$$

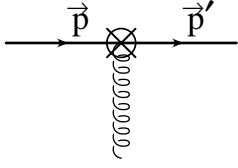


Time derivative vertex

$$\frac{-ie}{8m^2} q^0 (\vec{p}' + \vec{p}) \times \vec{\sigma}$$

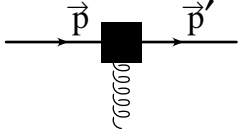
Figure 3 (continued)

Derivative Fermi vertices



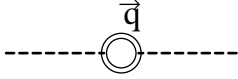
$$\frac{-ie}{8m^3}(\vec{p}'^2 + \vec{p}^2)(\vec{p}' - \vec{p}) \times \vec{\sigma}$$

$$\frac{-ie}{8m^3}\vec{q}^2(\vec{p}' - \vec{p}) \times \vec{\sigma}$$

 $p'p$  vertex

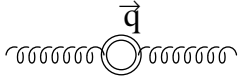
$$\frac{-ie}{8m^3}(\vec{p}' \times \vec{p})\vec{\sigma} \cdot (\vec{p}' + \vec{p})$$

cvp



$$\frac{-\vec{q}^4}{m^2}$$

tvp



$$\frac{\vec{q}^4}{m^2}(\delta^{ij} - \frac{q^i q^j}{\vec{q}^2})$$

Therefore, the remaining task for construction of the NRQED Hamiltonian is determination of the coefficients of these operators appearing in Eq. (19).

Let us first consider the QED diagram in which one photon is exchanged between the electron and the muon. The first step to obtain the “renormalization” coefficients of the operators in the NRQED Hamiltonian is to carry out nonrelativistic reduction of the QED scattering amplitude exchanging one photon between the electron and the muon. Comparing this QED scattering amplitude with the scattering amplitude derived from the general form of NRQED Lagrangian given in Eq. (19), we are able to fix the “renormalization” coefficient  $c_i$ ’s. We want to choose the simplest process to find them. It turns out that all “renormalization” coefficients in (19) can be obtained by using the external static potential. The comparison between the corresponding QED and NRQED amplitudes is shown in Fig.

4. We will work out nonrelativistic reduction of operators of order up to  $\alpha v^6$  and  $\alpha v^4$  for spin-flip and spin-non-flip ones, respectively. Since the spin-non-flip operators contribute to the hyperfine splitting only through the higher order bound state perturbation, we need only operators of order lower than the spin-flip ones. The QED scattering amplitude to be studied here consists of a tree vertex and one dressed by a radiative photon. Because we are dealing with the scattering amplitude, we also have a diagram with self-energy insertion on the external fermion lines. However, these diagrams can be dropped after the mass renormalization and wave function renormalization are carried out, if one chooses the on-shell renormalization scheme. Then the QED scattering amplitude is expressed by the usual form factors  $F_1$  and  $F_2$ .

For the external static vector potential  $\vec{A}(\vec{q})$ , we easily find the QED scattering amplitude

$$\begin{aligned}
& e\bar{u}(\vec{p}') \left[ -\vec{\gamma} \cdot \vec{A}(\vec{q}) F_1(q^2) + \frac{i}{2m} \sigma^{ij} A^i(\vec{q}) q^j F_2(q^2) \right] u(\vec{p}) \\
&= F_1(q^2) \psi^\dagger(\vec{p}') \left[ -\frac{e}{2m} (\vec{p}' + \vec{p}) \cdot \vec{A} - \frac{ie}{2m} \vec{\sigma} \cdot (\vec{q} \times \vec{A}) \right. \\
&\quad \left. + \frac{ie}{8m^3} (\vec{p}'^2 + \vec{p}^2) \vec{\sigma} \cdot (\vec{q} \times \vec{A}) + \dots \right] \psi(\vec{p}) \\
&\quad + F_2(q^2) \psi^\dagger(\vec{p}') \left[ -\frac{ie}{2m} \vec{\sigma} \cdot (\vec{q} \times \vec{A}) + \frac{ie}{16m^3} (\vec{p}'^2 + \vec{p}^2) \vec{\sigma} \cdot (\vec{q} \times \vec{A}) \right. \\
&\quad \left. + \frac{ie}{8m^3} \vec{\sigma} \cdot \vec{p}' \vec{\sigma} \cdot (\vec{q} \times \vec{A}) \vec{\sigma} \cdot \vec{p} + \dots \right] \psi(\vec{p}), \tag{33}
\end{aligned}$$

where  $u$  and  $\psi$  are Dirac and Pauli spinors, respectively. Similarly, for the external static Coulomb field  $A^0(\vec{q})$ , we have

$$\begin{aligned}
& e\bar{u}(\vec{p}') \left[ \gamma^0 A^0(\vec{q}) F_1(q^2) - \frac{i}{2m} \sigma^{0j} A^0(\vec{q}) q^j F_2(q^2) \right] u(\vec{p}) \\
&= F_1(q^2) \psi^\dagger(\vec{p}') \left[ eA^0 - \frac{e}{8m^2} \vec{q}^2 A^0 + \frac{ie}{4m^2} \vec{\sigma} \cdot (\vec{p}' \times \vec{p}) A^0 + \dots \right] \psi(\vec{p}) \\
&\quad + F_2(q^2) \psi^\dagger(\vec{p}') \left[ -\frac{e}{4m^2} \vec{q}^2 A^0 + \frac{ie}{2m^2} \vec{\sigma} \cdot (\vec{p}' \times \vec{p}) A^0 + \dots \right] \psi(\vec{p}). \tag{34}
\end{aligned}$$

Taking account of the fact that  $q^0$  is of order  $v^2$  and  $|\vec{q}|$  is of order  $v$ , the nonrelativistic expansion of the form factors can be written as [27]

$$\begin{aligned}
F_1(q^2) &= 1 - \frac{\alpha}{3\pi} \left[ \frac{\vec{q}^2}{m^2} \left( \ln \left( \frac{m}{\lambda} \right) - \frac{3}{8} \right) \right] + \mathcal{O}(\alpha v^4, \alpha^2 v^2) \\
F_2(q^2) &= a_e - \frac{\alpha}{\pi} \frac{\vec{q}^2}{12m^2} + \mathcal{O}(\alpha v^4, \alpha^2 v^2), \tag{35}
\end{aligned}$$

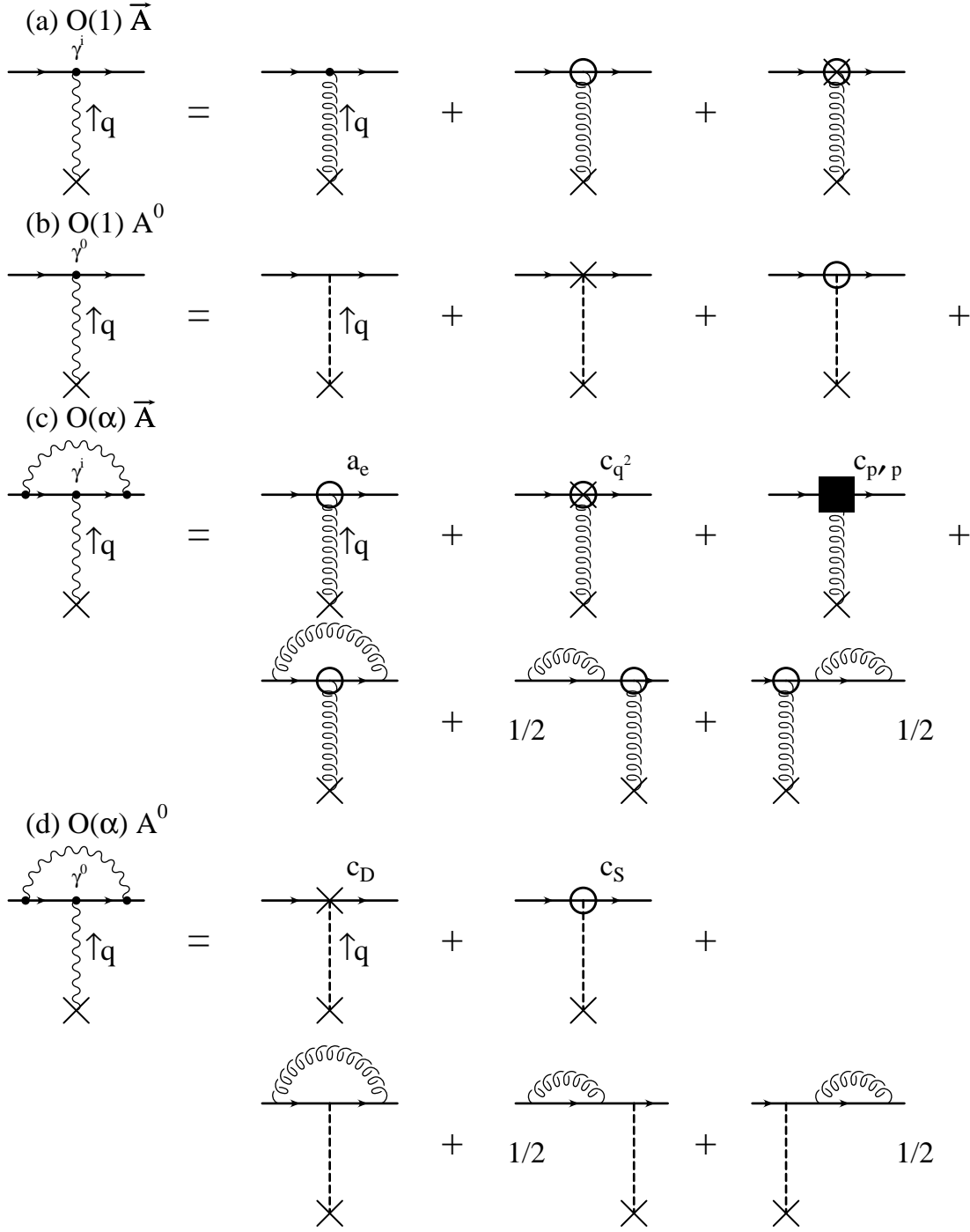


FIG. 4. QED and NRQED scattering diagram comparison. The diagrams on the left and right of the  $=$  sign represents QED and NRQED diagrams, respectively. The external fermions are on-the-mass-shell and at threshold. Self-energy diagrams coming from the  $\vec{A} \cdot \vec{A} \psi^\dagger \psi$  vertex as well as self-mass counterterms are not shown explicitly.

where  $a_e = F_2(0)$  is the anomalous magnetic moment of the electron.

Combining (33),(34) and (35) together, and comparing with the scattering amplitude derived from the NRQED Lagrangian given by (19), we find that the “renormalization” coefficients must be chosen as

$$\begin{aligned}
c_F^{QED} &= 1 + a_e, \\
c_D^{QED} &= 1 + \frac{\alpha}{\pi} \frac{8}{3} \left[ \ln \left( \frac{m}{\lambda} \right) - \frac{3}{8} \right] + 2a_e, \\
c_S^{QED} &= 1 + 2a_e, \\
c_{W1}^{QED} &= 1 + \frac{\alpha}{\pi} \frac{4}{3} \left[ \ln \left( \frac{m}{\lambda} \right) - \frac{3}{8} + \frac{1}{4} \right] + \frac{a_e}{2}, \\
c_{W2}^{QED} &= \frac{\alpha}{\pi} \frac{4}{3} \left[ \ln \left( \frac{m}{\lambda} \right) - \frac{3}{8} + \frac{1}{4} \right] + \frac{a_e}{2}, \\
c_{p'p}^{QED} &= a_e.
\end{aligned} \tag{36}$$

This procedure enables us to construct the NRQED Hamiltonian. However, it does not provide the complete NRQED Hamiltonian. One must also include terms which are the NRQED analogues of QED counterterms such as  $-\delta m \bar{u} u$ . To see this let us calculate the NRQED scattering amplitude which arises from the Coulomb term  $\psi^\dagger e A^0 \psi$  modified by a 1-loop NRQED radiative correction by a perturbative treatment of  $H_{\text{main}}$ .

The perturbation here means that the zeroth-order of NRQED Hamiltonian contains only the free part of the electron, and thus the Coulomb interaction is treated as perturbation. Some of these scattering amplitudes involving radiative corrections require new forms of the NRQED operators while others may be represented by additional “renormalization” constants of the already existing operators in  $H_{\text{main}}$ .

The fermion kinetic energy term in (19) gives the interaction term  $-\psi^\dagger e (\vec{p}' + \vec{p}) \cdot \vec{A} / (2m) \psi$  in the NRQED Hamiltonian. Note that, although the NRQED Hamiltonian is not an expansion into multipoles, we call this term the dipole interaction in the following for convenience's sake. Thus we consider the Coulomb term dressed by the transverse photon with the dipole couplings. The NRQED Feynman rule applied to this diagram gives

$$\psi^\dagger(\vec{p}') \left( \frac{e}{m} \right)^2 i \int^\Lambda \frac{d^4 k}{(2\pi)^4} \frac{1}{(k^0)^2 - \vec{k}^2 - \lambda^2 + i\epsilon} \left( \vec{p}' \cdot \vec{p} - \frac{\vec{p} \cdot \vec{k} \vec{p}' \cdot \vec{k}}{\vec{k}^2 + \lambda^2} \right)$$

$$\frac{1}{E + k^0 - (\vec{p}' + \vec{k})^2/(2m) + i\epsilon} eA^0 \frac{1}{E + k^0 - (\vec{p} + \vec{k})^2/(2m) + i\epsilon} \psi(\vec{p}). \quad (37)$$

We chose the contour in the upper half  $k^0$  plane to pick up only the negative energy photon pole. Then we neglect  $\vec{k}$  in the kinetic energy term  $(\vec{p} + \vec{k})^2/(2m)$  in the electron propagators. This is justified because the energy transfer between electrons is of order  $v^2$  when  $|\vec{p}|$  is of order  $v$ , while the space component of the photon momentum  $|\vec{k}|$  is of order  $v^2$ . After this approximation, angular integration over the photon momentum  $\vec{k}$  becomes trivial, leaving only the  $|\vec{k}|$  integration:

$$\begin{aligned} & \psi^\dagger(\vec{p}') \left( \frac{e}{m} \right)^2 \frac{2}{3} \vec{p}' \cdot \vec{p} \int_0^\Lambda \frac{dk}{2\pi^2} \frac{k^2}{2\sqrt{k^2 + \lambda^2}} \left( 1 + \frac{1}{2} \frac{\lambda^2}{k^2 + \lambda^2} \right) \\ & \frac{-2m}{\vec{p}'^2 - 2mE + 2m\sqrt{k^2 + \lambda^2}} eA^0 \frac{-2m}{\vec{p}^2 - 2mE + 2m\sqrt{k^2 + \lambda^2}} \psi(\vec{p}) \\ & = \psi^\dagger(\vec{p}') \frac{\alpha}{\pi} \frac{8}{3} \left[ \ln \left( \frac{2\Lambda}{\lambda} \right) - \frac{5}{6} \right] \frac{-e}{8m^2} (-2\vec{p}' \cdot \vec{p}) A^0 \psi(\vec{p}) + \mathcal{O}(v^8). \end{aligned} \quad (38)$$

In the last step, we used the on-shell, at-threshold condition,  $E = -\vec{p}'^2/(2m) + \mathcal{O}(v^4)$ .

The diagram with a self-energy on the external electron line gives

$$\begin{aligned} & \frac{1}{2} \psi^\dagger(\vec{p}') \left[ \frac{-2m}{\vec{p}'^2} \left( \frac{e}{m} \right)^2 \frac{2}{3} \vec{p}' \cdot \vec{p} \int_0^\Lambda \frac{dk}{2\pi^2} \frac{k^2}{2\sqrt{k^2 + \lambda^2}} \left( 1 + \frac{1}{2} \frac{\lambda^2}{k^2 + \lambda^2} \right) \frac{-2m}{\vec{p}^2 - 2mE} \right. \\ & \left. \left\{ \frac{-2m}{\vec{p}^2 - 2mE + 2m\sqrt{k^2 + \lambda^2}} - \frac{-1}{\sqrt{k^2 + \lambda^2}} \right\} eA^0 + (\vec{p} \rightarrow \vec{p}') \right] \psi(\vec{p}) \\ & = \psi^\dagger(\vec{p}') \frac{\alpha}{\pi} \frac{8}{3} \left[ \ln \left( \frac{2\Lambda}{\lambda} \right) - \frac{5}{6} \right] \frac{-e}{8m^2} (\vec{p}'^2 + \vec{p}^2) A^0 \psi(\vec{p}) + \mathcal{O}(v^8). \end{aligned} \quad (39)$$

Note that the term  $-1/\sqrt{k^2 + \lambda^2}$  is the “mass renormalization term” of NRQED.<sup>3</sup>

In order to maintain the equivalence of QED and NRQED we must include the negative of these contributions in  $H_{\text{main}}$ . (See Fig. 4(d).) From (38) and (39) we see that this is achieved by adding the new “renormalization” coefficients to the Darwin term  $-\psi^\dagger e \vec{q}^2 A^0 / (8m^2) \psi$ :

$$\psi^\dagger(\vec{p}') c_D^{NRQED} \frac{-e \vec{q}^2}{8m^2} A^0 \psi(\vec{p}), \quad (40)$$

---

<sup>3</sup>“Tadpole” diagram due to the  $\langle \vec{A} \cdot \vec{A} \psi^\dagger \psi \rangle$  completely vanishes after mass renormalization because this diagram does not depend on the external fermion momentum.



where

$$c_D^{NRQED} = \frac{\alpha}{\pi} \frac{8}{3} \left[ \ln \left( \frac{\lambda}{2\Lambda} \right) + \frac{5}{6} \right] . \quad (41)$$

The entire coefficient of the Darwin term is the sum of QED and NRQED contributions:

$$\begin{aligned} c_D &= c_D^{QED} + c_D^{NRQED} \\ &= 1 + \frac{\alpha}{\pi} \frac{8}{3} \left[ \ln \left( \frac{m}{2\Lambda} \right) - \frac{3}{8} + \frac{5}{6} \right] + 2a_e . \end{aligned} \quad (42)$$

Actually, this additional contribution from NRQED serves to eliminate the contribution of the longitudinal polarization associated with the finite photon mass [30]. In other words, the  $\ln \lambda$  term in the “renormalization” coefficients due to QED is effectively replaced in the NRQED “renormalization” constant by

$$\ln \lambda \rightarrow \ln(2\Lambda) - \frac{5}{6} . \quad (43)$$

Similarly the NRQED radiative correction to the Fermi term,  $-\psi^\dagger ie \vec{\sigma} \cdot (\vec{q} \times \vec{A}) / (2m) \psi$ , yields the correct “renormalization” coefficient of the  $W_1$  and  $W_2$  derivative Fermi terms,  $\psi^\dagger ie (\vec{p}'^2 + \vec{p}^2) \vec{\sigma} \cdot (\vec{q} \times \vec{A}) / (8m^3) \psi$  and  $\psi^\dagger ie (-2\vec{p}' \cdot \vec{p}) \vec{\sigma} \cdot (\vec{q} \times \vec{A}) / (8m^3) \psi$ , respectively, which are given by

$$\begin{aligned} c_{W_1} &= 1 + \frac{\alpha}{\pi} \frac{4}{3} \left[ \ln \left( \frac{m}{2\Lambda} \right) - \frac{3}{8} + \frac{1}{4} + \frac{5}{6} \right] + \frac{a_e}{2} , \\ c_{W_2} &= \frac{\alpha}{\pi} \frac{4}{3} \left[ \ln \left( \frac{m}{2\Lambda} \right) - \frac{3}{8} + \frac{1}{4} + \frac{5}{6} \right] + \frac{a_e}{2} . \end{aligned} \quad (44)$$

The radiative correction comes also from vacuum polarization. Since vacuum polarization is a highly virtual process within the framework of NRQED, no vacuum polarization term exists in  $H_{\text{main}}$ . Instead, its contribution is represented by the new photon interaction terms in NRQED. Again we begin with the nonrelativistic reduction of QED amplitude with one vacuum polarization insertion. QED gives the renormalized vacuum polarization tensor

$$\Pi^{\mu\nu}(q) = (q^\mu q^\nu - g^{\mu\nu} q^2) \Pi(q^2) , \quad (45)$$

with

$$\Pi(q^2) = -\frac{q^2}{m^2} \int_0^1 dt \frac{\rho(t)m^2}{q^2 - 4m^2(1-t^2)^{-1}} . \quad (46)$$

For the second order, the photon spectral function  $\rho_2(t)$  is known to be

$$\rho_2(t) = \frac{\alpha}{\pi} \frac{t^2(1 - \frac{1}{3}t^2)}{1 - t^2} . \quad (47)$$

Expanding  $\Pi(q^2)$  around  $q^2 = 0$ , we obtain

$$\Pi_2(q^2) = c_{\text{vp}} \frac{-\vec{q}^2}{m^2} + \mathcal{O}(\alpha v^4, \alpha^2 v^2) , \quad (48)$$

where

$$c_{\text{vp}} = \frac{\alpha}{15\pi} . \quad (49)$$

Thus, in the Coulomb gauge, two new photon interaction terms are added to the photon Hamiltonian

$$c_{\text{vp}} A^i(q) \frac{\vec{q}^4}{m^2} A^j(q) (\delta^{ij} - \frac{q^i q^j}{\vec{q}^2}) , \quad (50)$$

and

$$c_{\text{vp}} A^0(\vec{q}) \frac{-\vec{q}^4}{m^2} A^0(\vec{q}) . \quad (51)$$

## D. Photon-Fermion Scattering Amplitude

Let us now turn to the processes which contain two fermion operators and two external photons. To determine the “renormalization” coefficients we must carry out the nonrelativistic reduction of these QED scattering amplitudes. In practice, however, we don’t have to do it at all because the “renormalization” coefficients of these operators up to  $v^6$  for spin-flip ones and  $v^4$  for spin-non-flip ones are identical with those determined by the scattering amplitude due to a static external potential because of gauge invariance. For instance, the same “renormalization” coefficient  $c_S$  for the spin-orbit interaction term

$$\psi^\dagger \frac{ie}{4m^2} \vec{\sigma} \cdot (\vec{p}' \times \vec{p}) A^0 \psi \quad (52)$$

must be used for both the seagull term

$$\psi^\dagger \frac{-ie^2}{4m^2} \vec{\sigma} \cdot (\vec{q}_1 \times \vec{A}(q_1)) A^0(q_2) \psi \quad (53)$$

and the time derivative term

$$\psi^\dagger \frac{ie}{8m^2} q^0 \vec{\sigma} \cdot ((\vec{p}' + \vec{p}) \times \vec{A}) \psi. \quad (54)$$

The seagull term is the only operator involving two-photons relevant to our immediate interest. This contributes to the  $(Z\alpha)^2$  and  $\alpha(Z\alpha)^2$  corrections.

In general an explicit nonrelativistic reduction of the photon-fermion scattering amplitude is necessary only if one wants to find the “renormalization” coefficients of operators of higher order in  $v$ , such as  $\psi^\dagger \vec{E} \cdot \vec{E} \psi / m^3 \sim v^6$ .

We note that  $H_{\text{main}}$  is not an unique expression. Using the equation of motion for the fermion field, we can obtain another form of Hamiltonian. When  $H_{\text{main}}$  is quantized, we should be more careful. Use of the equation of motion is equivalent to the transformation of the electron field. We have to take into account the Jacobian of this change of variables. Once the Jacobian is taken into account, two Hamiltonians become completely identical and produce the same results even for the bound state calculation [25]. This is why we excluded the operators having time derivatives, such as  $\bar{\psi}(iD_t)^2\psi/m$ , from our consideration, since the equation of motion renders  $iD_t\psi$  to  $(\vec{p}^2/(2m) + \mathcal{O}(v^4))\psi$ .

In this manner we have obtained all operators in the main part of the NRQED Hamiltonian  $H_{\text{main}}$  necessary for our calculation to the desired order.

### E. The NRQED Hamiltonian $H_{\text{main}}$

For later reference let us write down the part of the NRQED Hamiltonian  $H_{\text{main}}$  valid to order  $\alpha$  by putting together the results of Sec. IIC and IID. To do this, we introduce the  $\vec{q}^2$  derivative Fermi term by combining the  $W_1$  and  $W_2$  derivative Fermi term at the order  $\alpha$ . It is of the form:

$$\begin{aligned}
H_{\text{main}}^\Lambda = \psi^\dagger(\vec{p}') \Bigg[ & \frac{\vec{p}^2}{2m} + eA^0 - \frac{(\vec{p}^2)^2}{8m^3} - \frac{e}{2m}(\vec{p}' + \vec{p}) \cdot \vec{A} + \frac{e^2}{2m} \vec{A} \cdot \vec{A} \\
& - \frac{ie}{2m} c_F \vec{\sigma} \cdot (\vec{q} \times \vec{A}) - \frac{e}{8m^2} c_D \vec{q}^2 A^0 \\
& + \frac{ie}{4m^2} c_S \vec{\sigma} \cdot (\vec{p}' \times \vec{p}) A^0 - \frac{ie^2}{4m^2} c_S \vec{\sigma} \cdot (\vec{q}_1 \times \vec{A}(q_1)) A^0(q_2) \\
& + \frac{ie}{8m^2} c_S q^0 \vec{\sigma} \cdot ((\vec{p}' + \vec{p}) \times \vec{A}) \\
& + \frac{ie}{8m^3} c_W (\vec{p}'^2 + \vec{p}^2) \vec{\sigma} \cdot (\vec{q} \times \vec{A}) + \frac{ie}{8m^3} c_{q^2} \vec{q}^2 \vec{\sigma} \cdot (\vec{q} \times \vec{A}) \\
& + \frac{ie}{8m^3} c_{p'p} \{ \vec{p} \cdot (\vec{q} \times \vec{A}) (\vec{\sigma} \cdot \vec{p}') + \vec{p}' \cdot (\vec{q} \times \vec{A}) (\vec{\sigma} \cdot \vec{p}) \} \\
& + \dots \Bigg] \psi(\vec{p}) \\
& + c_{\text{vp}} A^i(q) \frac{\vec{q}^4}{m^2} A^j(q) (\delta^{ij} - \frac{q^i q^j}{\vec{q}^2}) \\
& + c_{\text{vp}} A^0(\vec{q}) \frac{-\vec{q}^4}{m^2} A^0(\vec{q}) , \tag{55}
\end{aligned}$$

where  $\vec{p}'$  and  $\vec{p}$  are the outgoing and incoming fermion momenta, respectively, and  $q = (q^0, \vec{q})$  is the incoming photon momentum. In the seagull vertex,  $\vec{q}_1$  is the incoming momentum of the vector potential  $\vec{A}$ . The superscript  $\Lambda$  indicates that the Hamiltonian is regularized with the UV cut-off  $\Lambda$ . The “renormalization” coefficients are

$$\begin{aligned}
c_F &= 1 + a_e , \\
c_D &= 1 + \frac{\alpha}{\pi} \frac{8}{3} \left[ \ln \left( \frac{m}{2\Lambda} \right) - \frac{3}{8} + \frac{5}{6} \right] + 2a_e , \\
c_S &= 1 + 2a_e , \\
c_W &= 1 , \\
c_{q^2} &= \frac{\alpha}{\pi} \frac{4}{3} \left[ \ln \left( \frac{m}{2\Lambda} \right) - \frac{3}{8} + \frac{5}{6} + \frac{1}{4} \right] + \frac{a_e}{2} , \\
c_{p'p} &= a_e , \\
c_{\text{vp}} &= \frac{\alpha}{15\pi} . \tag{56}
\end{aligned}$$

Thus far we have not shown explicitly the contact term  $H_{\text{contact}}$  of the NRQED Hamiltonian, which is also obtained by comparison of the electron-muon scattering amplitudes in QED and NRQED. The explicit form of the contact term will be given in Sec. III and IV as we calculate  $\alpha(Z\alpha)$  and  $\alpha^2(Z\alpha)$  corrections, respectively, to the hyperfine splitting.

## F. Application of $H_{\text{main}}$ to Bound States

Let us now turn our attention to the bound state calculation using  $H_{\text{main}}$ . The main part of the NRQED Hamiltonian for the muon field is obtained by replacing the charge  $e$  by  $-Ze$  in the  $H_{\text{main}}$  for the electron field. For the nonrecoil hyperfine correction, only the Fermi and Coulomb terms are necessary in the muon Hamiltonian. Together with the photon Hamiltonian, we can construct various perturbative potentials appearing in the nonrelativistic Rayleigh-Schrödinger perturbation theory (26). The lowest order contribution  $E_F$  to hyperfine splitting comes from the Fermi potential (31). A survey of Eqs. (55) and (56) shows that the only order  $\alpha$  correction is  $a_e E_F$  which exhibits the effect of the “renormalization”:  $c_F - 1 = a_e$ . Other possible contributions to the hyperfine splitting coming from  $H_{\text{main}}$  are those of the first order perturbation of the derivative Fermi term and the seagull term, and the second order perturbation which involves the Fermi term and the  $p^4$  relativistic kinetic term or the Darwin term. The  $(p'^2 + p^2)$  derivative Fermi term leads to the potential of order  $(Z\alpha)^6(m/M)m$ :

$$V_W = -\frac{\pi Z\alpha}{mM} \frac{(\vec{p}'^2 + \vec{p}^2)}{4m^2} (\psi^\dagger \vec{q} \times \vec{\sigma}_e \psi) \cdot (\chi^\dagger \vec{q} \times \vec{\sigma}_\mu \chi) \frac{1}{(\vec{q}^2 + \lambda^2)}. \quad (57)$$

The Darwin term generates the potential of order  $(Z\alpha)^4 m$ :

$$V_D = \frac{4\pi Z\alpha}{8m^2} (\psi^\dagger \psi) (\chi^\dagger \chi) \frac{\vec{q}^2}{(\vec{q}^2 + \lambda^2)}. \quad (58)$$

Expectation values of these potentials with respect to the bound state wave function diverge due to integration over  $\vec{q}$ . This is why we need the help of the contact term  $H_{\text{contact}}$  for their cancellation. When the effect of  $H_{\text{contact}}$  is included, these four potentials together give the  $(Z\alpha)^2$  Breit correction. A detailed discussion about the treatment of these UV divergent operators is found in [10] where the derivation of the Breit  $(Z\alpha)^2$  correction from NRQED is described.

Similarly an  $\alpha(Z\alpha)^2$  correction is obtained when the contribution of the “renormalization” coefficients is included in each potential. Third order perturbation theory

in  $H_{\text{main}}$  with an intermediate radiative photon and dipole couplings also gives the  $\alpha(Z\alpha)^2$  correction. This is because these diagrams have the structure similar to the derivative Fermi term or the Darwin term as is shown in the determination of the “renormalization” coefficients in NRQED (See Eqs. (38) and (39)).

The additional photon interaction terms (50) and (51) due to vacuum polarization produce the effective potentials

$$V_{\text{tvp}} = \frac{\pi(Z\alpha)}{mM} c_{\text{vp}} \frac{\vec{q}^2}{m^2} (\psi^\dagger \vec{q} \times \vec{\sigma}_e \psi) \cdot (\chi^\dagger \vec{q} \times \vec{\sigma}_\mu \chi) \frac{\vec{q}^2}{(\vec{q}^2 + \lambda^2)^2} \quad (59)$$

and

$$V_{\text{cvp}} = -\frac{4\pi Z\alpha}{m^2} c_{\text{vp}} (\psi^\dagger \psi) (\chi^\dagger \chi) \frac{\vec{q}^4}{(\vec{q}^2 + \lambda^2)^2} . \quad (60)$$

We note that the first spin-flip potential  $V_{\text{tvp}}$  has exactly the same structure as the  $q^2$  derivative Fermi potential. Thus it contributes not to the order  $\alpha(Z\alpha)$  but to the order  $\alpha(Z\alpha)^2$ . The spin-non-flip potential  $V_{\text{cvp}}$  behaves as a  $\delta$  function potential in the coordinate space just like the Darwin potential. Thus it also contributes to the  $\alpha(Z\alpha)^2$  term through the second order perturbation theory.

To summarize, no order  $\alpha$  correction exists besides  $a_e E_F$ , where  $E_F$  is given by (32). In the NRQED formulation, it is transparent why only the anomalous magnetic moment of a *free* electron contributes to the order  $\alpha$  correction to  $E_F$ .

### III. THE $\alpha(Z\alpha)$ CORRECTION

In this section we show how the non-recoil radiative correction of order  $\alpha(Z\alpha)$ , calculated long ago by Kroll and Pollock and by Karplus, Klein and Schwinger [31], can be obtained within the framework of NRQED. For brevity, let us refer to this as the K-P term. The procedures developed here are readily applicable to the  $\alpha^2(Z\alpha)$  term calculation in NRQED.

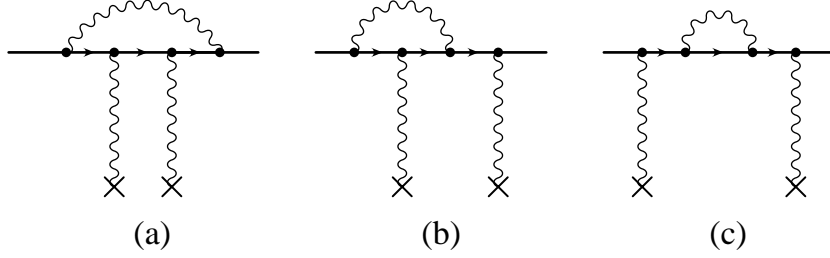


FIG. 5. QED diagrams contributing to the  $\alpha(Z\alpha)$  radiative correction to the muonium hyperfine splitting.

### A. Diagram Selection

The QED diagrams involved in this calculation are shown in Fig. 5. In the original and subsequent works [31,9,32,13], the K-P  $\alpha(Z\alpha)E_F$  pure radiative correction was evaluated from the QED diagrams with the external fermions put on the mass-shell and at the threshold, and multiplied by the square of the nonrelativistic Coulomb wave function at the origin. This recipe was justified after complicated and rigorous consideration of the relativistic bound state theory. We shall show that NRQED provides an alternative justification of this procedure in the sense that no other correction term is needed in this order.

The correction terms whose coefficients are odd powers of  $Z\alpha$  may arise only from very limited sources in the NRQED bound state theory. The NRQED Lagrangian  $L_{\text{main}}$  consists only of terms with even parity. This implies that the expectation values of these terms with respect to the Coulomb wave function are even in  $Z\alpha$ , the typical electron momentum of the Coulomb bound state being  $|\vec{p}| \sim (Z\alpha)m$ .

The odd power of  $Z\alpha$  in the K-P term  $\sim \alpha(Z\alpha)^5 m^2/M$  therefore implies that there is no contribution to it from the  $L_{\text{main}}$  part of the NRQED Lagrangian. [Note that the “renormalization” constant  $c_i$  in  $L_{\text{main}}$  does not depend on  $Z\alpha$ . (See Eq. (19) and Eq. (23)).]

This means that the correction we are looking for must come entirely from the NRQED contact terms of (22). To determine the contact term, we compare the scattering amplitudes

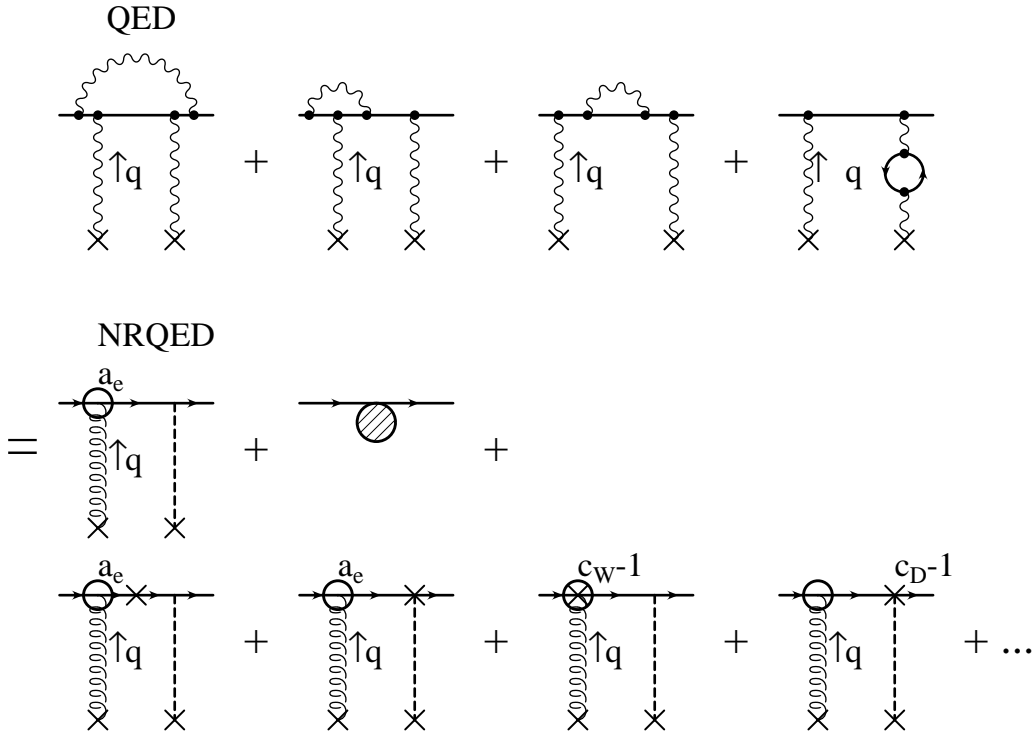


FIG. 6. QED and NRQED two-photon exchange scattering diagram comparison in the presence of the radiative correction. The shaded circle represents the contact term introduced in this comparison. The NRQED diagrams in the bottom lines actually contribute to the  $\alpha(Z\alpha)^2$  correction.

evaluated in NRQED and QED in the same power of explicit  $\alpha$  and  $Z\alpha$ . This comparison is shown in Fig. 6. For a given power of the coupling constant  $\alpha$ , the number of QED diagrams is finite while the number of NRQED diagrams is infinite. We terminate the series of NRQED scattering diagrams using the power counting rule for their contribution to the *bound* state.

We chose the electron mass  $m$  as the momentum scale of comparison, and evaluate the scattering amplitudes of both QED and NRQED on the mass-shell and at the threshold. In general, this procedure must be carried out for both spin-flipping and non-flipping amplitudes. However, for the K-P term, only the spin-flipping one is needed. The spin-non-flipping type produces a Lamb-shift type contact term, which contributes to the hyperfine splitting



only in the order  $\alpha(Z\alpha)^7 m^2/M$  and above.

As we have discussed in Sec. II, the comparison of QED and NRQED scattering amplitudes gives rise to a contact term to the NRQED Hamiltonian. We restrict ourselves to the consideration of the contact term relevant to the hyperfine splitting, i.e.,

$$\delta H = -d_1 \frac{1}{mM} (\psi^\dagger \vec{\sigma}_e \psi) \cdot (\chi^\dagger \vec{\sigma}_\mu \chi), \quad (61)$$

because this is the only source of the K-P term as was discussed above.

Let us first focus on the contribution from the vacuum polarization insertion. The two-photon exchange scattering amplitudes containing the vacuum polarization potential of (55) contributes to the order  $\alpha(Z\alpha)^2$ , not to  $\alpha(Z\alpha)$ . Thus the only contribution from the vacuum polarization is obtained from the contact term which is determined by calculating the QED two-photon exchange amplitude with one vacuum polarization insertion in the photon line with the on-shell at-threshold external fermions times the square of the Coulomb wave function at the origin.

Let us turn next to the contribution from the radiative photon. The QED diagrams related to this correction are shown in Fig. 5. All three QED scattering amplitudes have the same form:

$$i\mathcal{T}^{QED} = e^2 (Ze^2)^2 \int \frac{d^4 q}{(2\pi)^4} \frac{\bar{u}_e \mathcal{E}^{\mu\nu} u_e \bar{u}_m \mathcal{M}_{\mu\nu} u_m}{(q^2 + i\epsilon)^2}. \quad (62)$$

Here the electron factor  $\mathcal{E}^{\mu\nu}$  is different for each diagram but the muon factor  $\mathcal{M}_{\mu\nu}$  is common to all these diagrams and represents the sum of the ladder and crossed-ladder diagrams:

$$\mathcal{M}_{\mu\nu} = \frac{\gamma_\mu (\not{l} - \not{q} + M) \gamma_\nu}{(l - q)^2 - M^2 + i\epsilon} + \frac{\gamma_\nu (\not{l} + \not{q} + M) \gamma_\mu}{(l + q)^2 - M^2 + i\epsilon}, \quad (63)$$

where  $l = (M, \vec{0})$  is the external muon momentum and  $q$  is the four momentum flowing in the loop between the electron and the muon. As is well known [8], in the limit of infinite muon mass, the muon factor reduces to

$$\mathcal{M}_{\mu\nu} = \gamma_\nu \not{q} \gamma_\mu \frac{-2\pi i \delta(q^0)}{2M}. \quad (64)$$

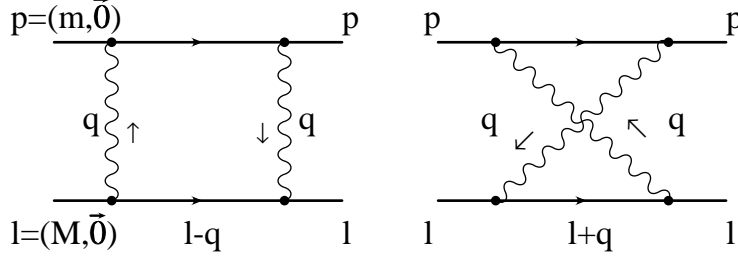


FIG. 7. Ladder and crossed-ladder diagrams.

This is represented by the symbol  $\times$  in Figs. 1, 2, 6, and 5.

The hyperfine splitting projection operator for strings of  $\gamma$  matrices is obtained by taking the difference between the  $J = 1, J_z = 0$  state and  $J = 0$  state and using the spherical symmetry of the system [33]:

$$\frac{1}{12} \sum_{i=1}^3 \text{Tr}[\mathcal{E}^{\mu\nu} \gamma^5 \gamma^i (\gamma^0 + 1)] \text{Tr}[\mathcal{M}_{\mu\nu} \gamma^5 \gamma_i (\gamma^0 + 1)] , \quad (65)$$

where Roman letters run from one to three while Greek letters run from zero to three. This projection is true only for external fermions on-the-mass-shell and at-threshold. The trace of the muon factor is easily taken, yielding

$$\epsilon_{\mu\nu ji} q^j \frac{-2\pi i \delta(q^0)}{2M} . \quad (66)$$

We take the  $\epsilon_{\mu\nu ji} q^j$  part together with the electron projection operator as the hfs projection operator, and the other muon factor will be included as a numerical factor.

In order that these diagrams contribute to the hyperfine splitting, one of the exchanged photons must be transverse (attached to a vertex  $\gamma^i$ ) while the other is Coulombic (attached to a vertex  $\gamma^0$ ). Our projection operator of hyperfine splitting picks up automatically this structure from the electron-line.

The corresponding NRQED scattering amplitude consists of many diagrams, but most of them actually contribute to the order higher than the K-P term. The only diagram necessary is a combination of the Fermi potential multiplied by the NRQED renormalization constant,

namely the second order anomalous magnetic moment, and the Coulomb potential. This scattering amplitude is named  $i\mathcal{T}^{NRQED}$ .

Other diagrams, such as the combination of the Darwin potential  $V_D$  including the “renormalization” constant and the Coulomb potential, have the same power of explicit  $\alpha$  and  $Z\alpha$  as the Fermi one, but diverges linearly in both UV and IR region. These divergences cancel out in the bound state calculation. The detail is similar to the discussion on the Breit term calculation given in [10]. Eventually they contribute to the terms of order  $\alpha(Z\alpha)^2$ . This argument holds also for the potentials  $V_{\text{vp}}$  and  $V_{\text{cvp}}$  representing the vacuum polarization effect.

The QED processes with three or more photon exchange contribute to obviously higher order terms due to the explicit extra power of the coupling constant  $Z\alpha$ .

The contact term can be defined as the QED amplitude minus the NRQED amplitude for the two photon exchange process:

$$-d_1 \frac{1}{mM} (\psi^\dagger \vec{\sigma}_e \psi) \cdot (\chi^\dagger \vec{\sigma}_\mu \chi) \equiv i\mathcal{T}^{QED} - i\mathcal{T}^{NRQED} . \quad (67)$$

Actually both QED and NRQED amplitudes are IR divergent in the limit of the vanishing external photon momentum  $\vec{q}$ . These threshold singularities cancel each other in the difference (67).

This contact term is to be put into the first order perturbation theory. Then the wave function integral is trivially done, resulting in the square of the Coulomb wave function at the origin. Thus the K-P term is given by

$$\Delta\nu(\text{KP}) = |\phi(0)|^2 \frac{-d_1}{mM} \langle \vec{\sigma}_e \cdot \vec{\sigma}_\mu \rangle \Big|_{J=0}^{J=1} , \quad (68)$$

where  $|\phi(0)|^2 = \gamma^3/\pi$  for the ground state. In the actual calculation, we take the difference between spin  $J=1$  and  $J=0$  for the scattering amplitude first using the projection operator.

## B. Calculation of the QED Amplitude

We have shown that the  $\alpha(Z\alpha)$  non-recoil radiative correction comes entirely from the NRQED contact term evaluated at the origin of the wave function. On the other hand, evaluation of the NRQED contact term is equivalent to that of the on-shell at-threshold QED scattering amplitude. This is why the calculation of the  $\alpha(Z\alpha)$  term is much simpler than other terms such as the  $\alpha(Z\alpha)^2$  term.

Our approach to carry out the computation of the QED scattering amplitudes is by numerical integration. Let us explain the outline of our procedure. The detail of the calculation is given in Appendix B. The electron-line structure of each diagram is directly written down using the parametric Feynman-Dyson rules for QED [34,35]. Feynman parameters assigned to the electron-line are  $z_1$ ,  $z_2$ , and  $z_3$ , while one assigned to the radiative photon line is  $z_4$ . The momenta flowing in the fermion lines after the radiative photon loop momentum is integrated out are expressed in terms of correlation functions  $B_{ij}$ , which are functions of Feynman parameters and determined by the topology of the loop structure of the diagram alone. Then our integrals are expressed as two or three dimensional Feynman-parametric integrals with an additional one dimension corresponding to the magnitude of the momentum  $\vec{q}$  of the external potential.

Two of the QED diagrams have UV divergences and must be renormalized. The renormalization terms are generated using the projection operators in the algebraic program FORM [36]. Our projection operators for QED renormalization constants are quite general and applicable to any order. They are presented in Appendix A. All of the renormalization constants are determined in the on-shell scheme. These renormalization terms should be expressed by the same Feynman parameters as those assigned to the original diagrams in order to realize point-by-point subtraction in numerical integration by means of the adaptive iterative Monte-Carlo integration routine VEGAS [37].

The hfs contribution due to the second order anomalous magnetic moment should be subtracted from the diagrams involving the second order vertex correction. Actually it is

very easily done along with the charge renormalization: Let the external photon momentum  $\vec{q}$  tend to zero in the original diagram expression of the electron factor. Then subtract this IR limit from the original diagram. We can easily prove that this IR limit of the diagram is nothing but the sum of the charge renormalization constant and the anomalous magnetic moment of the second order. (See [10] for details.)

Even though all diagrams are free from UV divergences after the renormalization is completed, they still suffer from IR divergence. In general, the Coulomb bound state has two kinds of IR divergence: one is due to the threshold singularity, and the other is due to the radiative photon.

The mechanism of threshold singularity is the following. In order to contribute to the hyperfine splitting, one of the two exchanged photons must be Coulomb-like while the other is transverse. This Coulomb photon may be absorbed in the wave function. As a result, the diagram is reduced to one of lower order in  $Z\alpha$ , or multiplied by  $1/(Z\alpha)$ . This is the physical origin of this type of IR divergence, which is ubiquitous in the relativistic treatment of bound state problem. In the calculation of the  $\alpha(Z\alpha)$  correction, however, such a “divergence” can be avoided completely by subtracting the contribution of the free anomalous magnetic moment. This is because other threshold singularities are absent due to the on-shell renormalization.

The remaining IR singularity is caused by radiative photons. Our choice to deal with this singularity is to put a small photon mass  $\lambda$  in the radiative photon. For the K-P term, this singularity must cancel out when all QED diagrams of the gauge invariant set are included.

### **C. Summary of the $\alpha(Z\alpha)$ Correction**

We have shown that non-recoil radiative corrections to the muonium hyperfine splitting having the odd power of  $Z\alpha$  comes only from the contact term of NRQED, and that this contact term is determined as the difference between the QED and NRQED scattering amplitudes.

The resulting expression for the K-P radiative correction can be evaluated either analytically or numerically. We have chosen the later approach. The three dimensional integration has been carried out using the adaptive iterative Monte-Carlo integration routine VEGAS [37]. Each diagram has the IR divergence of the form proportional to  $\sqrt{m/\lambda}$ , but their sum is finite. Our numerical evaluation shows that the contribution due to the radiative photon is given by

$$\Delta\nu(\text{KP})_{\text{ph}} = -2.556\ 80(6)\alpha(Z\alpha)E_F. \quad (69)$$

We have also evaluated this integral analytically and obtained the same result as that of Kroll and Pollock, and Karplus, Klein, and Schwinger [31]:

$$\Delta\nu(\text{KP})_{\text{ph}} = \left(\ln 2 - \frac{13}{4}\right)\alpha(Z\alpha)E_F = (-2.556\ 852\cdots)\alpha(Z\alpha)E_F. \quad (70)$$

An easy analytic calculation of the vacuum-polarization contribution gives

$$\Delta\nu(\text{KP})_{\text{VP}} = \frac{3}{4}\alpha(Z\alpha)E_F. \quad (71)$$

Putting these results together we obtain the well known  $\alpha(Z\alpha)$  correction in the frame work of NRQED:

$$\Delta\nu(\text{KP}) = \left(\ln 2 - \frac{13}{4} + \frac{3}{4}\right)\alpha(Z\alpha)E_F. \quad (72)$$

This justifies the procedure adopted in Ref. [31].

## IV. THE $\alpha^2(Z\alpha)$ CORRECTION

### A. Diagram Selection

In this section, we give an outline of the evaluation of the  $\alpha^2(Z\alpha)$  correction to the Fermi frequency  $E_F$  which comes from the six gauge invariant sets of QED Feynman diagrams represented by Fig. 1. Our treatment of the bound state to find the contribution to hyperfine splitting coming from these diagrams is completely identical with that of the  $\alpha(Z\alpha)$  K-P

correction. A new diagram appearing in this order is the light-by-light scattering insertion. The light-by-light scattering is a high energy process in NRQED. Thus it is represented only by a contact term in NRQED. As a result we have to include the four-photon interaction in the NRQED Hamiltonian. But as an operator it contributes to orders higher than our interest here. Therefore, what to do is again to calculate the contact term starting from the scattering amplitudes of these diagrams with the on-shell at-threshold particles and then subtract the contribution of the fourth order anomalous magnetic moment from Figs. 1(d) and 1(f).

The numerical evaluation of Fig. 1 (a) – (e) can be carried out easily and our results are consistent with those previously obtained by Eides and his collaborators [20–22]. In contrast, the diagrams of Fig. 1 (f) require a substantial effort to compute. A complete evaluation of this contribution is the main result of this paper.

## B. Calculation of the QED Amplitude

Let us now discuss some technical details of calculation of (17) represented by the nineteen diagrams of Fig. 2. Since the bound state structure of these diagrams is identical with that of the  $\alpha(Z\alpha)$  correction, the procedure of numerical evaluation of the  $\alpha(Z\alpha)$  correction given in Appendix B can be applied readily to these diagrams. We applied numerous techniques developed for the numerical calculation of the anomalous magnetic moment  $g - 2$  of the electron [35], except that we avoided the use of “intermediate” renormalization which was introduced in the  $g - 2$  calculation to avoid the IR singularity of each diagram. Instead we use the conventional renormalization procedure which is IR singular in the radiative photon mass  $\lambda$ . This is because these IR divergent terms are needed to cancel out the other IR singularity, the threshold singularity in the vanishing external photon momentum  $\vec{q} = 0$ , in the proper diagram. The detail of this mechanism is described in the calculation of the  $\alpha(Z\alpha)$  K-P correction in Appendix B.

It is convenient to divide the nineteen diagrams into four groups:

Group 1: Diagrams containing fourth-order vertex corrections. They are represented by the diagrams  $H_{01}, H_{02}, H_{03}, H_{09}, H_{10}$  and  $H_{11}$  of Fig. 2.

Group 2: Diagrams containing fourth-order self-energy insertions. They are represented by the diagrams  $H_{04}, H_{12}$  of Fig. 2.

Group 3: Diagrams in which radiative photons span over two external photons. They are represented by the diagrams  $H_{05}, H_{06}, H_{07}, H_{08}, H_{13}, H_{14}, H_{15}$ , and  $H_{16}$  of Fig. 2.

Group 4: Diagrams containing two non-overlapping second-order radiative corrections. They are represented by the diagrams  $H_{17}, H_{18}$ , and  $H_{19}$  of Fig. 2.

The integrands corresponding to the individual diagrams of Fig. 2 were initially generated using the algebraic program SCHOONSCHIP [38]. Later we generated the same integrands by FORM [36] as a check.

The parametric representation of Group 1 diagrams is of the form

$$\frac{3}{32} \frac{\alpha^2(Z\alpha)}{\pi} E_F \frac{m}{\pi^2} \int_0^\infty \frac{dq}{\vec{q}^2} \mathbf{F}_1^\mu \int \frac{(dz)_{1-4}}{U^2} \frac{1}{V^2} \left[ \frac{\not{p} + \not{q} + 1}{-\vec{q}^2} \right] \gamma^\nu, \quad (73)$$

where the diagram  $H_{01}$ , for example, has the electron-line operator

$$\mathbf{F}_1^\mu = \gamma^\alpha (\not{D}_1 + m) \gamma^\beta (\not{D}_2 + m) \gamma_\beta (\not{D}_3 + m) \gamma^\mu (\not{D}_4 + m) \gamma_\alpha. \quad (74)$$

Other diagrams of this group are obtained by permutation of  $\gamma$  matrices. (See Ref. [35] for the definition of  $U$ ,  $V$ ,  $D_i$ , etc.) Using the hyperfine splitting projection operator, one finds that the terms contributing to the hyperfine splitting are proportional to at least  $\vec{q}^2$ , and kills one of the  $\vec{q}^2$ 's in the denominator in Eq. (73). Thus Eq.(73) leads to the energy shift of the form

$$\Delta\nu_{G1} = \frac{\alpha^2(Z\alpha)}{\pi} E_F \frac{m}{\pi^2} \int_0^\infty \frac{dq}{(-\vec{q}^2)} \int \frac{(dz)_{1-4}}{U^2} \left[ \frac{F_0}{V^2} + \frac{F_1}{UV} + \frac{F_2}{U^2 V^0} \right], \quad (75)$$

where  $1/V^0$  is a symbolical representation of  $-\ln V$  in which the UV divergence is regularized and subtracted by the corresponding counterterm. (See Appendix B for a precise definition.)

The parametric representation of Group 2 diagrams is of the form

$$-\frac{3}{32} \frac{\alpha^2(Z\alpha)}{\pi} E_F \frac{m}{\pi^2} \int_0^\infty \frac{dq}{\vec{q}^2} \gamma^\mu \left[ \frac{\not{p} + \not{q} + m}{-\vec{q}^2} \right] \mathbf{F}_2 \int \frac{(dz)_{2-4}}{U^2} \frac{1}{V} \left[ \frac{\not{p} + \not{q} + m}{-\vec{q}^2} \right] \gamma^\nu, \quad (76)$$



where, for example, the diagram  $H_{04}$  has the electron-line operator

$$\mathbf{F}_2 = \gamma^\alpha (\not{D}_2 + m) \gamma^\beta (\not{D}_3 + m) \gamma_\beta (\not{D}_4 + m) \gamma_\alpha . \quad (77)$$

Its contribution to the hyperfine splitting has the form

$$\Delta\nu_{G2} = \frac{\alpha^2(Z\alpha)}{\pi} E_F \frac{m}{\pi^2} \int_0^\infty \frac{dq}{(-\vec{q}^2)^2} \int \frac{(dz)_{2-4}}{U^2} \left[ \frac{F_0}{V} + \frac{F_1}{UV^0} \right] . \quad (78)$$

For the diagrams  $H_{04}$  and  $H_{12}$ , the product of two electron propagators just outside the fourth order self-energy diagram behave as  $(1/\vec{q}^2)^2$ , which makes the convergence of the numerical integrals difficult in the small  $|\vec{q}|$  region, even though the integrals are analytically free from the IR singularity in  $|\vec{q}|$  after the mass and wave function renormalizations are carried out. In order to avoid this computational difficulty, we introduced an additional parameter  $y$  varying from zero to one to combine the original term and the renormalization term. All the numerator expressions are then proportional to at least  $\vec{q}^2$  and kills one of the electron propagators.

The parametric representation of Group 3 is of the form

$$- \frac{3}{16} \frac{\alpha^2(Z\alpha)}{\pi} E_F \frac{m}{\pi^2} \int_0^\infty \frac{dq}{\vec{q}^2} \mathbf{F}_3^{\mu,\nu} \int \frac{(dz)_{1-5}}{U^2} \frac{1}{V^3} . \quad (79)$$

For instance, the diagram  $H_{05}$  has the electron-line operator  $\mathbf{F}_3^{\mu,\nu}$ :

$$\mathbf{F}_3^{\mu,\nu} = \gamma^\alpha (\not{D}_1 + m) \gamma^\beta (\not{D}_2 + m) \gamma_\beta (\not{D}_3 + m) \gamma^\mu (\not{D}_4 + m) \gamma^\nu (\not{D}_5 + m) \gamma_\alpha . \quad (80)$$

By using the hyperfine splitting projection operator, we get

$$\Delta\nu_{G3} = \frac{\alpha^2(Z\alpha)}{\pi} E_F \frac{m}{\pi^2} \int_0^\infty dq \int \frac{(dz)_{1-5}}{U^2} \left[ \frac{F_0}{V^3} + \frac{F_1}{UV^2} + \frac{F_2}{U^2V} \right] . \quad (81)$$

The Group 4 diagrams  $H_{17}$ ,  $H_{18}$ , and  $H_{19}$  contain two non-overlapping second-order radiative corrections. Their sum is invariant under the covariant gauge transformation and free from the IR singularity due to the radiative photons.

Let us consider the sum of two diagrams of Fig. 8. If the photon propagator is chosen as

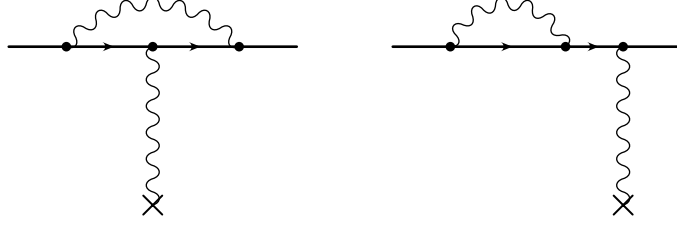


FIG. 8. Sum of the second-order self-energy diagram and vertex diagram.

$$\frac{-i}{k^2 + i\epsilon} (g^{\mu\nu} - \beta \frac{k^\mu k^\nu}{k^2}) , \quad (82)$$

the gauge-dependent part of the vertex diagram gives

$$\begin{aligned} & \beta \int^\Lambda \frac{d^4 k}{(2\pi)^4} \not{k} \frac{i}{\not{p} - \not{k} + \not{q} - m} \gamma^\mu \frac{i}{\not{p} - \not{k} - m} \not{k} \frac{-i}{k^2} \\ & = i\beta \int^\Lambda \frac{d^4 k}{(2\pi)^4 k^2} \not{k} \frac{1}{\not{p} - \not{k} + \not{q} - m} \gamma^\mu (-1) , \end{aligned} \quad (83)$$

where we use the on-shell condition  $\not{p} = m$ . The self-energy diagram with one external photon diagram is

$$\begin{aligned} & \beta \int^\Lambda \frac{d^4 k}{(2\pi)^4} \not{k} \frac{i}{\not{p} - \not{k} + \not{q} - m} \not{k} \frac{i}{\not{p} + \not{q} - m} \gamma^\mu \frac{-i}{k^2} \\ & = i\beta \int^\Lambda \frac{d^4 k}{(2\pi)^4 k^2} \not{k} \left[ \frac{1}{\not{p} - \not{k} + \not{q} - m} \gamma^\mu - \frac{1}{\not{p} + \not{q} - m} \gamma^\mu \right] . \end{aligned} \quad (84)$$

The second term, which is related to the mass renormalization constant proportional to the longitudinal photon polarization, vanishes when the integration over  $k$  is carried out with a proper regularization. Then the gauge dependent parts of (83) and (84) cancel each other and the sum is independent of particular choice of gauge.

The numerical integration is performed for the integral combining three diagrams  $H_{17}$ ,  $H_{18}$  and  $H_{19}$  together so that cancellation of IR divergences occurs in the same region of the Feynman parametric space. The result obtained for the zero mass radiative photon ( $\lambda^2 = 0$ ) is

$$\Delta\nu(H_{17}) + \Delta\nu(H_{18}) + \Delta\nu(H_{19}) = -0.478\,03\,(15) \frac{\alpha^2(Z\alpha)}{\pi} E_F . \quad (85)$$

This is in good agreement with the result calculated in the Fried-Yennie gauge [40], in which  $\beta = -2$  in (82),

$$\Delta\nu(H_{17}) + \Delta\nu(H_{18}) + \Delta\nu(H_{19}) = -0.477\,89\,(1)\frac{\alpha^2(Z\alpha)}{\pi}E_F. \quad (86)$$

Note that  $\Delta\nu(H_{17})$ ,  $\Delta\nu(H_{18})$ , and  $\Delta\nu(H_{19})$  individually are gauge dependent, and their values are completely different between our results and those of Ref. [40].

### C. Problems Concerning Numerical Integration

Let us now discuss some technical details of calculation of  $\Delta\nu(H_{01})$  to  $\Delta\nu(H_{16})$ . After the ultraviolet divergences are renormalized, individual diagrams still suffer from severe infrared (IR) divergence, which is of the form  $\lambda^{-1/2}$ ,  $\lambda$  being the photon rest mass measured in units of the electron mass. Of course, the sum over all diagrams of Fig. 2 is free from the IR divergence. This does not mean, however, that the sum can be integrated easily on a computer. This is because the IR finiteness results from cancellation of divergences for  $\lambda \rightarrow 0$  from different parts of the integration domain.

One way to deal with this problem is to evaluate individual integrals for several small values of  $\lambda$  and extrapolate the sum of all terms to zero photon mass. Unfortunately, this approach creates integrals of order  $10^3$  for  $\lambda^2 \sim 10^{-7}$ , while their sum is of order 1, making it very difficult to control the numerical accuracy of the result. Another way is to integrate, for  $\lambda \neq 0$ , the sum of all terms, which enables us to avoid dealing directly with large numbers. This approach will also result in a better error estimate. The main practical difficulty is the large amount of computing time required.

This problem can be somewhat alleviated if one evaluates each integral after subtracting its IR-divergent part, and then evaluates the sum  $\mathcal{S}$  of the IR-subtraction terms of all diagrams. This method, which we have chosen, ensures that all integrals stay small (less than  $\sim 20$ ) for any value of  $\lambda$ . Thus far, we have evaluated them for several values of  $\lambda^2$  in the range of  $10^{-3}$  to  $10^{-7}$ . The integration has been carried out numerically using

Table II: Vegas integration performed for individual diagrams of Fig. 2.  $\mathcal{S}$  is the sum of IR divergent parts of diagrams  $H_{01}$  through  $H_{16}$ .  $\lambda$  is the photon mass measured in units of the electron mass.

	$\lambda^2 = 10^{-3}$	$\lambda^2 = 10^{-3.5}$	$\lambda^2 = 10^{-4}$	$\lambda^2 = 10^{-4.5}$	$\lambda^2 = 10^{-5}$	$\lambda^2 = 10^{-5.5}$	$\lambda^2 = 10^{-6}$	$\lambda^2 = 10^{-7}$
$H_{01}$	-4.9551(4)	-5.5548(4)	-6.0481(4)	-6.4490(4)	-6.7714(5)	-7.0304(4)	-7.2360(4)	-7.5298(4)
$H_{02}$	0.0950(1)	0.3601(2)	0.6337(1)	0.8976(2)	1.1402(2)	1.3565(2)	1.5443(2)	1.8398(2)
$H_{03}$	-6.5527(4)	-7.5536(5)	-8.4213(5)	-9.1585(6)	-9.7758(5)	-10.2877(4)	-10.7089(4)	-11.3314(4)
$H_{04}$	1.6048(1)	1.9811(2)	2.3670(2)	2.7574(3)	3.1487(3)	3.5389(3)	3.9266(3)	4.6937(3)
$H_{05}$	4.0899(4)	4.6116(5)	5.0464(6)	5.3997(5)	5.6836(6)	5.9083(5)	6.0833(5)	6.3199(6)
$H_{06}$	-3.4781(5)	-3.8533(5)	-4.2074(6)	-4.5364(6)	-4.8346(6)	-5.1006(4)	-5.3326(4)	-5.7030(6)
$H_{07}$	1.2588(3)	1.2690(3)	1.2426(3)	1.1898(3)	1.1176(4)	1.0318(3)	0.9361(3)	0.7263(4)
$H_{08}$	-0.2167(0)	-0.2980(1)	-0.3677(1)	-0.4255(1)	-0.4721(1)	-0.5092(1)	-0.5380(1)	-0.5775(1)
$H_{09}$	0.0059(2)	-0.3047(2)	-0.5929(2)	-0.8486(2)	-1.0682(2)	-1.2528(2)	-1.4061(2)	-1.6333(2)
$H_{10}$	7.7184(3)	9.1640(4)	10.4746(5)	11.6210(5)	12.5985(6)	13.4159(4)	14.0900(4)	15.0840(6)
$H_{11}$	-1.8437(2)	-2.4663(3)	-3.0333(3)	-3.5309(3)	-3.9559(3)	-4.3127(3)	-4.6078(3)	-5.0457(4)
$H_{12}$	4.4780(3)	5.4636(4)	6.3444(5)	7.1092(5)	7.7567(5)	8.2968(4)	8.7423(4)	9.4015(6)
$H_{13}$	-3.2369(3)	-3.6631(4)	-4.0220(5)	-4.3157(6)	-4.5505(5)	-4.7339(4)	-4.8732(4)	-5.0485(5)
$H_{14}$	-3.6981(2)	-4.3597(2)	-4.9672(3)	-5.5084(3)	-5.9802(3)	-6.3839(3)	-6.7246(3)	-7.2437(4)
$H_{15}$	-1.9611(2)	-2.5301(2)	-3.0774(2)	-3.5843(2)	-4.0403(3)	-4.4414(2)	-4.7882(3)	-5.3325(4)
$H_{16}$	-1.5242(1)	-1.7852(1)	-2.0058(2)	-2.1863(2)	-2.3307(2)	-2.4442(2)	-2.5325(1)	-2.6519(4)
$H_{17}, H_{18}, H_{19}$	-0.4780(1)							
$\mathcal{S}$	8.2098(17)	9.4538(21)	10.5296(27)	11.4341(31)	12.1829(36)	12.7885(55)	13.2507(104)	13.8516(186)
TOTAL	-0.4840(20)	-0.5436(25)	-0.5828(31)	-0.6128(35)	-0.6295(40)	-0.6381(57)	-0.6526(105)	-0.6585(186)

FIG. 9. The graph for the coefficient  $y$  of  $E_F\alpha^2(Z\alpha)/\pi$  obtained by VEGAS versus  $x \equiv \lambda^{\frac{1}{2}}$ . The solid line is the chi-square fit for  $y = a_0 + a_1x + a_2x^2$ , where  $a_0, a_1$ , and  $a_2$  are determined from the data listed in Table I.

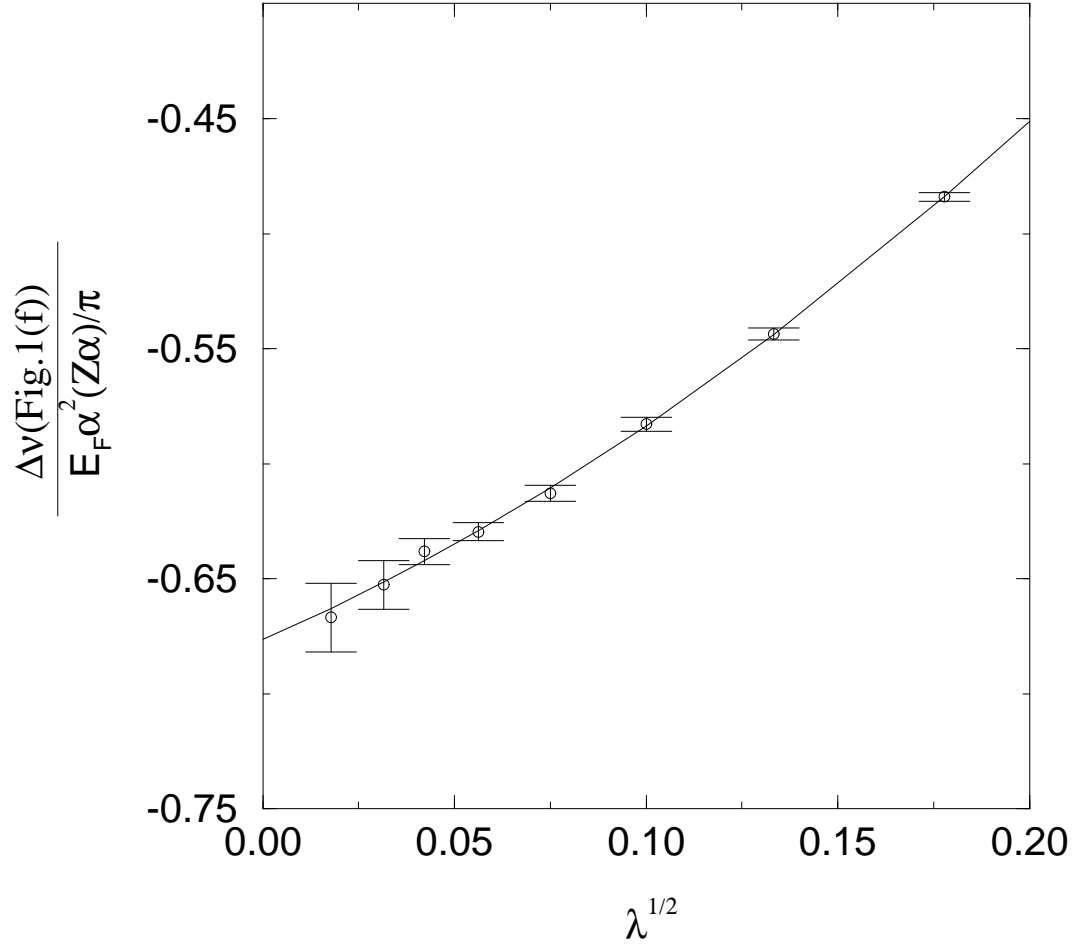


TABLE III. The chi-square fitting for the coefficient  $y$  of  $E_F \alpha^2(Z\alpha)/\pi$  versus  $x \equiv \lambda^{\frac{1}{2}}$  where  $y = a_0 + a_1 x^2 + \dots$  and  $\lambda$  is the photon mass measured in units of the electron mass.

photon mass $\lambda^2$		$y = a_0 + a_1 x$	$y = a_0 + a_1 x + a_2 x^2$	$y = a_0 + a_1 x + a_2 x^2 + a_3 x^3$
$10^{-7} \leq \lambda^2 \leq 10^{-5}$	$a_0$	$-0.678 \pm 0.015$	$-0.700 \pm 0.041$	—
	$a_1$	$0.88 \pm 0.29$	$2.03 \pm 2.05$	—
	$a_2$	—	$-13.77 \pm 24.06$	—
$10^{-7} \leq \lambda^2 \leq 10^{-3}$	$a_0$	—	$-0.6764 \pm 0.0079$	$-0.672 \pm 0.017$
	$a_1$	—	$0.73 \pm 0.15$	$0.58 \pm 0.57$
	$a_2$	—	$1.99 \pm 0.63$	$3.45 \pm 5.62$
	$a_3$	—	—	$-4.39 \pm 16.78$

the adaptive iterative Monte-Carlo integration routine VEGAS [37]. The result of each integration is summarized in Table II. The degree of difficulty of numerical integration for  $\mathcal{S}$  increases rapidly as  $\lambda$  decreases. This prevents us from going to smaller values of  $\lambda$  at present. Even  $\lambda^2 = 10^{-7}$  is a struggle. Although evaluation of integrals up to  $\lambda^2 = 10^{-8}$  is highly desirable, we have not attempted it thus far since it will require an extraordinary amount of computing time.

The data in Table II shows that the contribution of Fig. 1(f) falls within errors on a straight line for  $10^{-7} \leq \lambda^2 \leq 10^{-5}$ . Thus the extrapolation to  $\lambda = 0$  may be tried with a linear polynomial  $a_0 + a_1 x$ , where  $x = \lambda^{1/2}$  [39]. The upper box of column 3 of Table III shows the best linear fit to the data in this range of  $\lambda$ .

We also list in the upper box of column 4 a fit to the same set of data in terms of a quadratic polynomial  $a_0 + a_1 x + a_2 x^2$ . Clearly the result is much less certain than the linear fit. This is because the increased flexibility of the quadratic polynomial is now responding not only to the nonlinearity of data but also to the noise of numerical integration. For this reason the fitting with a linear polynomial will be more appropriate for this data.

On the other hand, if one tries to fit the entire data of Table II which show clear deviation

from linearity, the linear fit is no longer appropriate and one must use (at least) a quadratic polynomial (See Fig. 9). The best fit by a quadratic polynomial to the whole set of data of Table II is shown in the bottom box of column 4. The bottom box of column 5 shows that use of a cubic polynomial is not recommended to this data because it responds more to the noise of numerical integration than to the real signal. Based on these considerations we believe that the value of  $a_0$  determined by the quadratic fit gives the best estimate of  $\Delta\nu(\text{Fig.1(f)})$ :

$$\Delta\nu(\text{Fig.1(f)}) = -0.676 \text{ 4 (79)} \frac{\alpha^2(Z\alpha)}{\pi} E_F . \quad (87)$$

## V. DISCUSSION

The remaining uncertainty in the value of  $\Delta\nu(\text{Fig.1(f)})$  is still considerable. Nevertheless it is a factor 5 improvement over the preliminary value (16). Since we published the preliminary result, Eides *et. al.* [40,41] have completed their calculation and reported a more accurate value

$$\begin{aligned} \Delta\nu(\text{Fig.1(f)}) &= -0.671 \text{ 1 (7)} \frac{\alpha^2(Z\alpha)}{\pi} E_F \\ &= -0.370 \text{ 1 (4)} \text{ kHz.} \end{aligned} \quad (88)$$

Our new result (87) is in close agreement with the result of Ref. [41]. Note that the calculation of Ref. [41] is carried out in the Fried-Yennie gauge while our work is carried out in the Feynman gauge. Considerably higher precision of (88) over (87) reflects the advantage of calculation in the Fried-Yennie gauge which renders each diagram IR-divergence-free when it is transformed by application of integration by part. This approach requires nontrivial amount of diagram-specific manipulation because of very complicated integrands involving many variables. In the Feynman gauge calculation, on the other hand, each diagram is IR divergent due to the retarded Coulomb-like photons, which makes individual integral cutoff dependent. The advantage of this approach is that one can apply a systematic computer

algebraic method, which minimizes the chance of making mistakes – an important consideration in such a complicated calculation. The agreement of (87) and (88) confirms gauge independence of the result to the extent of numerical precision.

The total contribution of order  $\alpha^2(Z\alpha)$  including the results (11)–(15) and (87) is given in (18). If we instead use (88) for Fig. 1(f), the total contribution becomes

$$\begin{aligned}\Delta\nu(\text{Fig.1}) &= 0.773\,2\,(7)\frac{\alpha^2(Z\alpha)}{\pi}E_F \\ &= 0.426\,4\,(4)\,\text{kHz}.\end{aligned}\tag{89}$$

If we add the  $\alpha(Z\alpha)^2$  correction to the previous theoretical prediction (10), we obtain

$$\Delta\nu(\text{new theory}) = \begin{cases} 4\,463\,302.69\,(1.34)\,(0.21)\,(0.16)\,\text{kHz} & \text{Eq.(18),} \\ 4\,463\,302.70\,(1.34)\,(0.21)\,(0.16)\,\text{kHz} & \text{Eq.(89).} \end{cases}\tag{90}$$

Now that the complete  $\alpha^2(Z\alpha)$  correction has been evaluated, the major remaining source of theoretical uncertainty in the muonium hyperfine structure is, as is seen from (4), the numerically evaluated nonlogarithmic part of the  $\alpha(Z\alpha)^2$  correction term. In addition, although not listed in (90), the leading logarithmic corrections of order  $\alpha^4$  and  $\alpha^3(m/M)$  turn out to contribute to the hyperfine structure as much as the  $\alpha^2(Z\alpha)$  term, as was shown in our preliminary report [3] and also by Karshenboim [42]. The parts of these higher order terms evaluated thus far add up to  $-0.68\,(6)\,\text{kHz}$  if some errors in [3] and [10] are corrected. (Details will be discussed in subsequent papers.) We cannot simply add these corrections to (90), however, because the previous evaluation of  $\alpha(Z\alpha)^2$  term [23] contains parts which are of higher order in  $Z\alpha$ . We have evaluated the  $\alpha(Z\alpha)^2$  and  $\alpha(Z\alpha)^3$  terms separately in the NRQED formalism in order to avoid possible double counting and reduce the uncertainties due to these terms. The results will be reported in the subsequent papers.

## ACKNOWLEDGMENTS

We thank G. P. Lepage, P. Labelle, late D. R. Yennie, P. Mohr and B. N. Taylor for useful discussions. Thanks are due to M. I. Eides for communicating their preliminary result. This



research is supported in part by the U. S. National Science Foundation. Part of numerical work was conducted at the Cornell National Supercomputing Facility, which receives major funding from the US National Science Foundation and the IBM Corporation, with additional support from New York State and members of the Corporate Research Institute.

## APPENDIX A: PROJECTION OPERATORS FOR QED RENORMALIZATION CONSTANTS

We present the projection operators for QED renormalization constants determined by the on-shell scheme. Our projection operators for QED renormalization constants are quite general and correct for any loop orders. We set the electron mass  $m = 1$  through Appendices A and B.

The projection operator of vertex renormalization terms can be written as [35]

$$L = \frac{1}{4} Tr[\Gamma_0(\gamma^0 + 1)], \quad (A1)$$

where  $\Gamma_\mu$  is the proper vertex diagram. Projection operators of mass renormalization term and wave function renormalization terms can be defined similarly. A proper self energy diagram of the  $2n$ -th order has the parametric representation

$$\Sigma^{(2n)} = -\left(\frac{-\alpha}{4\pi}\right)^n (n-2)! \mathbf{F} \int (dz)_G \frac{1}{U^2 V^{n-1}}. \quad (A2)$$

(See Ref. [35] for the definition of  $U$ ,  $V$ ,  $\mathbf{F}$ , etc.) The projection to the mass renormalization is given by

$$\begin{aligned} \delta m &= \frac{1}{4} Tr[\Sigma(p)(\not{p} + 1)]|_{p=1} \\ &= \left(\frac{\alpha}{\pi}\right)^n \int \frac{(dz)_G}{U^2} \sum_{m=0}^{n-1} \frac{F_m}{U^m V^{n-1-m}}, \end{aligned} \quad (A3)$$

where  $\Sigma(p)$  is defined by (A2). The projection operator of the wave function renormalization constant is slightly more complicated since it involves the derivative of the self energy with respect to the external momentum, namely  $p^\mu \partial \Sigma(p) / \partial p^\mu$ . It can be easily realized, however,

in the Feynman parametric representation. Taking the derivative of the numerator with respect to  $p$  leads to the quantity

$$\mathbf{E} = \sum_{\text{electron line only}} A_i \mathbf{F}_i . \quad (\text{A4})$$

where  $\mathbf{F}_i$  is obtained by replacing  $(\mathcal{D}_i + 1)$  by  $\not{p}$  in the electron-line operator  $\mathbf{F}$ . The corresponding part of the wave function renormalization constant is determined as

$$\begin{aligned} B_2(\text{numer.}) &= -\left(\frac{-\alpha}{4\pi}\right)^n (n-2)! \frac{1}{4} \text{Tr}[\mathbf{E}(\mathbf{p}) \not{p}(\not{p} + 1)]|_{p^2=1} \int (dz)_G \frac{1}{U^2 V^{n-1}} \\ &= \left(\frac{\alpha}{\pi}\right)^n \int \frac{(dz)_G}{U^2} \sum_{m=0}^{n-1} \frac{E_m}{U^m V^{n-1-m}} . \end{aligned} \quad (\text{A5})$$

The other part corresponding to the derivative of the denominator is similar to the mass renormalization  $\delta m$  and is given by

$$B_2(\text{denom.}) = \left(\frac{\alpha}{\pi}\right)^n \int \frac{(dz)_G}{U^2} \sum_{m=0}^{n-1} \frac{(n-1-m) 2 G F_m}{U^m V^{n-m}}, \quad (\text{A6})$$

where

$$\begin{aligned} G &= -\frac{1}{2} p^\nu \frac{\partial V}{\partial p^\nu} \Big|_{p^2=1} \\ &= \sum_{\text{electron line only}} z_i A_i . \end{aligned} \quad (\text{A7})$$

## APPENDIX B: NUMERICAL CALCULATION OF THE $\alpha(Z\alpha)$ CORRECTION

Let us begin by showing the calculation of the spanning photon diagram of Fig. 5(a). The Feynman parameters assigned to the electron-lines are  $z_1, z_2$ , and  $z_3$  and assigned to the radiative photon is  $z_4$ . Following the notation in Ref. [34,35], we use the abbreviation for the sum of Feynman parameters

$$z_{12\dots n} \equiv z_1 + z_2 + \dots + z_n . \quad (\text{B1})$$

For this diagram,  $z_{1234} = 1$ . The momentum flowing through each electron-line after integration of photon loop momentum should be expressed by the external momenta, namely

the electron momentum  $p = (m, \vec{0})$  and the momentum of the external potential  $q = (0, \vec{q})$ . For the electron-line  $i$ , this may be written as

$$Q'_i = A_i p + A_{iq} q, \quad (\text{B2})$$

where the “scalar” currents  $A_i$  and  $A_{iq}$  are found to be

$$\begin{aligned} A_1 = A_2 = A_3 = 1 - z_{123}U^{-1}, \quad A_{1q} = A_{3q} = -z_2U^{-1}, \\ A_{2q} = 1 + A_{1q}, \quad U = z_{1234} = 1. \end{aligned} \quad (\text{B3})$$

Then the electron-line including all of numerical factors is obtained in the operator form

$$\frac{3}{8} \frac{1}{\vec{q}^2} [(\mathcal{D}_1 + 1) \gamma^\mu (\mathcal{D}_2 + 1) \gamma^\nu (\mathcal{D}_3 + 1)] \int \frac{(dz)_{1-4}}{U^2} \frac{1}{V^2}, \quad (\text{B4})$$

where the  $i$ -th electron line operator  $D_i$  is

$$D_i^\mu = \frac{1}{2} \int_{m_i^2}^{\infty} dm_i^2 \frac{\partial}{\partial q_{i\mu}}. \quad (\text{B5})$$

Multiplying with the hyperfine splitting projection operator and taking the trace, we obtain the integrand as the FORM output [36]:

$$\begin{aligned} f(\vec{q}) = & 4 A_{1q}^2 A_{2q} \vec{q}^2 V^{-2} + (-4 A_1^2 A_{2q} + 8 A_{1q} - 4 A_{2q}) V^{-2} \\ & + B_{12} (8 A_{1q} + 4 A_{2q}) (UV)^{-1}, \end{aligned} \quad (\text{B6})$$

where

$$B_{12} = B_{23} = B_{31} = 1, \quad V = z_{123} - z_{123} A_1 + z_4 \lambda^2 + \vec{q}^2 z_2 A_{2q}. \quad (\text{B7})$$

The contribution to the hyperfine splitting energy is obtained as an integral of the form

$$\Delta E_1 = \alpha(Z\alpha) E_F \frac{1}{\pi^2} \int_0^\infty dq \int \frac{(dz)_{1-4}}{U^2} f(\vec{q}), \quad (\text{B8})$$

where

$$(dz)_{1-4} = dz_1 dz_2 dz_3 dz_4 \delta(1 - z_{1234}), \quad (\text{B9})$$

and  $f(\vec{q})$  is given by (B6).

Next consider the vertex correction diagram of Fig. 5(b). Feynman parameters  $z_1$  and  $z_2$  are assigned to the electron lines and  $z_4$  to the photon line, with the constraint  $z_{124} = 1$ .

The scalar currents are

$$A_1 = A_2 = 1 - z_{12}U^{-1}, \quad A_{2q} = -z_2U^{-1}, \quad A_{1q} = 1 + A_{2q}, \quad U = z_{124} = 1 \quad (\text{B10})$$

Then the electron-line is

$$-\frac{3}{8} \frac{1}{\vec{q}^2} [(\not{D}_1 + 1) \gamma^\mu (\not{D}_2 + 1) \gamma^\nu (\not{p} + \not{q} + 1)] \int_{\lambda^2}^{\Lambda^2} z_4 dm_4^2 \int \frac{(dz)_{124}}{U^2} \frac{1}{V^2}. \quad (\text{B11})$$

The integrand is found to be

$$\begin{aligned} f(\vec{q}) = & -4 A_{1q} A_{2q} \vec{q}^2 V^{-2} + (-4 - 4 A_1 A_{2q} + 4 A_1 A_{1q} + 8 A_1) V^{-2} \\ & + B_{12}(-4)(UV)^{-1}, \end{aligned} \quad (\text{B12})$$

where

$$B_{12} = 1, \quad V = z_{12} - z_{12} A_1 + z_4 \lambda^2 + \vec{q}^2 z_2 A_{2q}. \quad (\text{B13})$$

As was described in Sec. III, the charge renormalization and subtraction of the second order anomalous magnetic moment is carried out by subtracting  $f(\vec{q} = 0)$ . The hyperfine splitting contribution from two diagrams of the vertex type is

$$\Delta E_2 = \alpha(Z\alpha)E_F \frac{2}{\pi^2} \int_0^\infty \frac{dq}{(-\vec{q}^2)} \int_{\lambda^2}^{\Lambda^2} z_4 dm_4^2 \int \frac{(dz)_{124}}{U^2} [f(\vec{q}) - f(0)]. \quad (\text{B14})$$

If the  $m_4^2$  integral is performed, the denominator  $V^{-2}$  becomes  $V^{-1}$ . The  $V^{-1}$  term is UV divergent and, if it is combined with the charge renormalization term, it becomes  $-\ln V$ . In the self-energy diagram calculation, the regularization is implicitly performed and the resulting denominators are expressed by  $V^{-n}$ ,  $n = 0, 1, 2, \dots$ , where  $V^{-0}$  implies  $-\ln V$ .

The last diagram is the self-energy insertion diagram of Fig. 5(c). Feynman parameter  $z_2$  is assigned to the electron-line and  $z_4$  to the photon line with the constraint  $z_{24} = 1$ . The scalar currents are

$$A_2 = 1 - z_2 U^{-1}, \quad A_{2q} = A_2, \quad U = z_{24} = 1. \quad (\text{B15})$$

Then the electron-line is

$$\frac{3}{8} \frac{1}{\vec{q}^2} [(\not{p} + \not{q} + 1) \gamma^\mu (\not{D}_2 + 1) \gamma^\nu (\not{p} + \not{q} + 1)] \int \frac{(dz)_{24}}{U^2} \frac{1}{V}, \quad (\text{B16})$$

where

$$V = z_2 - z_2 A_2 + z_4 \lambda^2 + \vec{q}^2 z_2 A_{2q}. \quad (\text{B17})$$

The integrand is found to be

$$f(\vec{q}) = (-16 + 8 A_2 - 4 A_2 \vec{q}^2)(-\ln(V)). \quad (\text{B18})$$

The mass and wave function renormalization terms can be written as

$$f_R = G(16 - 8 A_2) \vec{q}^2 V_0^{-1} + (-16 + 8 A_2 - 4 A_2 \vec{q}^2)(-\ln(V_0)), \quad (\text{B19})$$

where

$$G = z_2 A_2, \quad V_0 = z_2 - z_2 A_2 + z_4 \lambda^2. \quad (\text{B20})$$

The hyperfine splitting contribution is given by

$$\Delta E_3 = \alpha(Z\alpha) E_F \frac{1}{\pi^2} \int_0^\infty \frac{dq}{(-\vec{q}^2)^2} \int \frac{(dz)_{24}}{U^2} [f(\vec{q}) - f_R]. \quad (\text{B21})$$

Although this integral is analytically free from the IR singularity caused in the limit of the vanishing external photon momentum  $\vec{q}$ , numerical integration is very difficult in the small  $q$  region, resulting in the poor convergence of the integral. To avoid this numerical difficulty, we introduce another parameter  $y$  varying from zero to one and combine the term which is not proportional to  $\vec{q}^2$  in the original diagram and the corresponding renormalization term together. This leads to an integrand of the form

$$\tilde{f}(\vec{q}) = G(16 - 8 A_2) \vec{q}^2 V_y^{-1} - 4 A_2 \vec{q}^2 (-\ln(V)), \quad (\text{B22})$$

where

$$V_y = z_2 - z_2 A_2 + z_4 \lambda^2 + \vec{q}^2 y z_2 A_{2q} . \quad (\text{B23})$$

The corresponding renormalization term is

$$\tilde{f}_R = G(16 - 8 A_2)\vec{q}^2 V_0^{-1} - 4 A_2 \vec{q}^2 (-\ln(V_0)) . \quad (\text{B24})$$

The resulting hyperfine splitting contribution is

$$\Delta E_3 = \alpha(Z\alpha)E_F \frac{1}{\pi^2} \int_0^\infty \frac{dq}{(-\vec{q}^2)^2} \int_0^1 dy \int \frac{(dz)_{24}}{U^2} [\tilde{f}(\vec{q}) - \tilde{f}_R] . \quad (\text{B25})$$

## REFERENCES

- [1] F. G. Mariam *et al.*, Phys. Rev. Lett. **49**, 993 (1982); E. Klempt *et al.*, Phys. Rev. D **25**, 652 (1982).
- [2] V. W. Hughes and G. zu Putlitz, Comm. Nucl. Part. Phys. **12**, 259 (1984).
- [3] T. Kinoshita and M. Nio, Phys. Rev. Lett. **72**, 3803 (1994).
- [4] E. Fermi, Z. Phys. **60**, 320 (1930).
- [5] W. E. Caswell and G. P. Lepage, Phys. Lett. B **167**, 437 (1986).
- [6] T. Kinoshita and G. P. Lepage, in *Quantum Electrodynamics*, ed. by T. Kinoshita (World Scientific, Singapore, 1990), pp. 81 - 89.
- [7] P. Labelle, G. P. Lepage, and U. Magnea, Phys. Rev. Lett. **72**, 2006 (1994).
- [8] J. R. Sapirstein and D. R. Yennie, in *Quantum Electrodynamics*, ed. by T. Kinoshita (World Scientific, Singapore, 1990), pp. 560 - 672.
- [9] S. J. Brodsky and G. W. Erickson, Phys. Rev. **148**, 26 (1966).
- [10] M. Nio, Ph.D. Thesis, Cornell University, August (1995).
- [11] Private communication from J. R. Sapirstein, 1995.
- [12] S. M. Schneider, W. Greiner and G. Soff, Phys. Rev. A **50**, 118 (1994).
- [13] M. I. Eides, S. G. Karshenboim, and V. A. Shelyuto, Phys. Lett. B **177**, 425 (1988); **202**, 572 (1988); M. I. Eides, S. G. Karshenboim, and V. A. Shelyuto, Ann. Phys. **205**, 231 (1991); **205**, 291 (1991).
- [14] M. I. Eides, S. G. Karshenboim, and V. A. Shelyuto, Phys. Lett. B **216**, 405 (1989); M. I. Eides and V. A. Shelyuto, Phys. Lett. B **146**, 241 (1984).
- [15] A. Karimkhodzhaev and R. N. Faustov, Yad. Fiz. **53**, 1012 (1991) [Eng. transl.: Sov. J. Nucl. Phys. **53**, 626 (1991)].

- [16] M. A. B. Bég and G. Feinberg, Phys. Rev. Lett. **33**, 606 (1974); G. T. Bodwin and D. R. Yennie, Phys. Rep. **43C**, 267 (1978).
- [17] M. A. B. Bég and G. Feinberg, Phys. Rev. Lett. **35**, 130(E) (1974).
- [18] M. E. Cage et al., IEEE Trans. Instrum. Meas., IM-38, 284 (1989).
- [19] F. Nez *et al.*, Phys. Rev. Lett. **69**, 2326 (1992); M. Weitz *et al.*, Phys. Rev. Lett. **72**, 328 (1994).
- [20] M. I. Eides, S. G. Karshenboim, and V. A. Shelyuto, Phys. Lett. B **229**, 285 (1989); **249**, 519 (1990).
- [21] M. I. Eides, S. G. Karshenboim, and V. A. Shelyuto, Yad. Fiz. **55**, 466 (1992) [Eng. transl.: Sov. J. Nucl. Phys. **55**, 257 (1992)]; Phys. Lett. B **268**, 433 (1991); Phys. Lett. B **316**, 631(E) (1993).
- [22] M. I. Eides, S. G. Karshenboim, and V. A. Shelyuto, Phys. Lett. B **319**, 545(E) (1993).
- [23] J. R. Sapirstein, Phys. Rev. Lett. **51**, 985 (1983).
- [24] H. Persson, S. M. Schneider, W. Greiner, G. Soff, and I. Lindgren, Gesellschaft für Schwerionenforschung preprint, GSI-95 (1995), to be published in Phys. Rev. Lett.
- [25] G. P. Lepage, L. Magnea, C. Nakhleh, U. Magnea, and K. Hornbostel, Phys. Rev. D **46**, 4052 (1992).
- [26] J. Schwinger, J. Math. Phys. **5**, 1606 (1964).
- [27] R. P. Feynman, Phys. Rev. **76**, 769 (1949).
- [28] D. A. Zwanziger, Phys. Rev. **121**, 1128 (1961).
- [29] Private communication from P. Labelle.
- [30] J. French and V. Weisskopf, Phys. Rev. **75**, 1240 (1949).



- [31] N. Kroll and F Pollock, Phys. Rev. **84**, 594 (1951), Phys. Rev. **86**, 876 (1952); R. Karplus, A. Klein, and J. Schwinger, Phys. Rev. **84** 597 (1951).
- [32] J. R. Sapirstein, E. A. Terray, and D. R. Yennie, Phys. Rev. Lett. **51**, 982 (1983); Phys. Rev. **D29**, 2290 (1984).
- [33] W. E. Caswell and G. P. Lepage, Phys. Rev. Lett. **41** 1092 (1978).
- [34] P. Cvitanovic and T. Kinoshita, Phys. Rev. D **10**, 3978 (1974).
- [35] T. Kinoshita, in *Quantum Electrodynamics*, ed. by T. Kinoshita (World Scientific, Singapore, 1990), pp. 218 - 321.
- [36] J. Vermaseren, Version 1.1, (1992).
- [37] G. P. Lepage, J. Comput. Phys. **27**, 192 (1978).
- [38] M. J. G. Veltman, 68000 Version, (1989).
- [39] W. H. Press, B. P. Flannery, S. A. Teukolsky, and W. T. Vetterling, *Numerical Recipes* (Cambridge University Press, 1989)
- [40] M. I. Eides, S. G. Karshenboim, and V. A. Shelyuto, Phys. Lett. B **312**, 358 (1993); Yad. Fiz. **57**, 1240 (1994); M. I. Eides, S. G. Karshenboim, and V. A. Shelyuto, Yad. Fiz. **57**, 2158 (1994).
- [41] M. I. Eides and V. A. Shelyuto, Pis'ma v ZhETP **61**, 465 (1995) [ JETP Lett. **61** 478 (1995)] ; Phys. Rev. A **52**, 954 (1995).
- [42] S. G. Karshenboim, Zh. Eksp. Teor. Fiz. **103**, 1105 (1993) [Eng. transl.: JETP **76**, 541 (1993)]; S. G. Karshenboim, preprint (1995), to be published in Zeitschrift für Physik D.